

# The binary fractions in the massive young Large Magellanic Cloud star clusters NGC 1805 and NGC 1818

Chengyuan Li<sup>1,2,3\*</sup>, Richard de Grijs<sup>1,2</sup> and Licai Deng<sup>3</sup>

<sup>1</sup>*Kavli Institute for Astronomy and Astrophysics, Peking University, Yi He Yuan Lu 5, Hai Dian District, Beijing 100871, China*

<sup>2</sup>*Department of Astronomy, Peking University, Yi He Yuan Lu 5, Hai Dian District, Beijing 100871, China*

<sup>3</sup>*Key Laboratory for Optical Astronomy, National Astronomical Observatories, Chinese Academy of Sciences, 20A Datun Road, Chaoyang District, Beijing 100012, China*

31 October 2018

## ABSTRACT

Using high-resolution data sets obtained with the *Hubble Space Telescope*, we investigate the radial distributions of the F-type main-sequence binary fractions in the massive young Large Magellanic Cloud star clusters NGC 1805 and NGC 1818. We apply both an isochrone-fitting approach and  $\chi^2$  minimization using Monte Carlo simulations, for different mass-ratio cut-offs,  $q$ , and present a detailed comparison of the methods' performance. Both methods yield the same radial binary fraction profile for the same cluster, which therefore supports the robustness and applicability of either method to young star clusters which are as yet unaffected by the presence of multiple stellar populations. The binary fractions in these two clusters are characterized by opposite trends in their radial profiles. NGC 1805 exhibits a decreasing trend with increasing radius in the central region, followed by a slow increase to the field's binary-fraction level, while NGC 1818 shows a monotonically increasing trend. This may indicate dominance of a more complicated physical mechanism in the cluster's central region than expected a priori. Time-scale arguments imply that early dynamical mass segregation should be very efficient and, hence, likely dominates the dynamical processes in the core of NGC 1805. Meanwhile, in NGC 1818 the behavior in the core is probably dominated by disruption of soft binary systems. We speculate that this may be owing to the higher velocity dispersion in the NGC 1818 core, which creates an environment in which the efficiency of binary disruption is high compared with that in the NGC 1805 core.

**Key words:** galaxies: star clusters – Magellanic Clouds – stars: binaries: general, close

## 1 INTRODUCTION

Characterization of the binary fractions in star clusters is of fundamental importance for many fields in astrophysics. Observations indicate that the majority of stars are found in binary systems (Duquennoy & Mayor 1991; Griffin & Suchkov 2003; Halbwegs et al. 2003; Kouwenhoven et al. 2005; Rastegaev 2010), while it is generally accepted that most stars with masses greater than  $0.5 M_{\odot}$  are formed in star clusters (Lada & Lada 2003). In addition, since binaries are on average more massive than single stars, in resolved star clusters these systems are thought to be good tracers of (dynamical) mass segregation. Over time, dynamical evolution through two-body relaxation will cause the most massive objects to migrate to the cluster centre, while the relatively lower-mass objects remain in or

migrate to orbits at greater radii (de Grijs et al. 2002a,b,c). This process will globally dominate a cluster's stellar distribution. However, close encounters involving binary systems may disrupt 'soft' (i.e., generally wide) binaries (Heggie 1975; Ivanova et al. 2005; Trenti et al. 2007a; Parker et al. 2009; Kaczmarek et al. 2011; de Grijs et al. 2013). This process will occur more frequently in a cluster's central, dense region than in its periphery, which may mask the effects of mass segregation. In the possible presence of intermediate-mass black holes in cluster cores, this dynamical scenario will proceed even more rapidly (Trenti et al. 2007b).

Young massive clusters are good targets to explore the early observational signatures of both (early) dynamical mass segregation and binary disruption, particularly since old clusters have already experienced significant evolution and their member stars will likely have reached a dynamical state close to energy equipartition. Although the Milky Way hosts a small number of young massive ( $\gtrsim 10^5 M_{\odot}$ )

\* E-mail: joshuali@pku.edu.cn

clusters, such as Westerlund 1, these objects are not suitable to explore these issues in detail. The rather extreme reddening associated with Westerlund 1 and other young, intermediate-mass clusters near the Galactic Centre prevents us from sampling significant numbers of their member stars in sufficient detail. This makes the young clusters in the Large Magellanic Cloud (LMC) interesting in this context. However, because the components of binary systems in massive, crowded star clusters at the distance of the LMC cannot be resolved with current instruments, binary fractions in distant, young massive clusters have not yet been studied as thoroughly as those in their older Galactic counterparts.

A number of approaches have been developed to analyse binary fractions in clusters. One of these aims at identifying binaries by measuring their radial velocity variability (Mateo 1996), but this method is only sensitive to bright stars because of spectroscopic limits, and it is affected by a strong detection bias towards short-period binaries. Another approach explores the photometric variability of cluster members. However, this method is also biased towards binaries with short periods (Milone et al. 2012) and the relatively high orbital inclinations required to observe at least partial eclipses, which cause variability. Both approaches are hampered by low discovery efficiencies, since they require extensive time-domain observations and, hence, significant allocations of telescope time.

A promising alternative method is based on statistical analysis of cluster colour–magnitude diagrams (CMDs). Unresolved binaries will be found on the brighter and redder side of the single-star main sequence (MS). Their importance can be quantified through careful Monte Carlo-type analysis. This approach can potentially yield a high detection efficiency, since it only depends on a single set of observations. In principle, one does not need to adopt many physical assumptions either; the approach is only based on our understanding of stellar evolution. This also allows us to simulate artificial observations for comparison, without having to rely on too many detailed physical considerations, such as regarding the period distribution of the binaries or their orbital inclinations (Rubenstein & Baylin 1997; Zhao & Baylin 2005; Sollima et al. 2007, 2010; Milone et al. 2012). However, almost all clusters which have been analysed based on the latter method are old stellar systems, in which dynamical evolution is expected to have significantly altered the initial binary population. Efforts have recently begun to address this issue in the context of the much more distant, young massive clusters in the LMC (Elson et al. 1998; Hu et al. 2010, 2011; de Grijs et al. 2013).

In this paper, we analyse the binary-fraction properties of two young massive LMC clusters, NGC 1805 and NGC 1818. Previous studies of these clusters have reported that both are significantly mass-segregated (e.g., de Grijs et al. 2002a,b,c). Elson et al. (1998), Hu et al. (2010) and de Grijs et al. (2013) studied the properties of the binary systems in NGC 1818; although Elson et al. (1998) reported apparent evidence of ‘binary segregation’ of the most massive binary systems in the cluster, de Grijs et al. (2013) found the opposite effect. In this paper, we explore the binary properties in both clusters in much more detail, while for NGC 1818 in particular we reduce the previously reported uncertainty ranges signifi-

cantly. We first analyse their CMDs to estimate the ratio of the number of possible binaries to the total stellar sample in the same magnitude range, simply based on assessment of the best-fitting isochrones and the expected photometric colour spread. We have also developed a more sophisticated and more accurate approach based on  $\chi^2$  minimization using Monte Carlo simulations. We will show that both methods lead to the same result for the same cluster, although the  $\chi^2$  minimization is preferred because it is physically better justified.

This paper is organized as follows. The data reduction is discussed in Section 2. The details of the isochrone-fitting and  $\chi^2$ -minimization methods are described in Sections 3 and 4, respectively. We also discuss and show how well either method performs. We go well beyond the approaches taken in previous studies of our target clusters. We have updated and significantly improved our analysis method with respect to that employed in de Grijs et al. (2013). We also take the possible effects of fast stellar rotation into consideration and show that the results remain robust, even if rapidly rotating stars were to contribute significantly to the clusters’ CMDs. We discuss the detailed physical implications of our results, as well as any possible shortcomings of the methods applied, in Section 5 and conclude the paper in Section 6.

## 2 DATA REDUCTION

The data sets pertaining to NGC 1805 and NGC 1818 were obtained from *Hubble Space Telescope* (HST) programme GO-7307 (PI Gilmore). The complete data set for a given cluster is composed of a combination of three Wide Field and Planetary Camera-2 (WFPC2) images in the F555W and F814W filters, which roughly correspond to the Johnson–Cousins *V* and *I* bands, respectively, with total exposure times of 2935 s and 3460 s. Both data sets consist of long- and short-exposure pointings in which the Planetary Camera (PC) chip was centred on the cluster centre region (referred to as our ‘CEN’ fields), with a third, longer-exposure image centred on the cluster’s half-light radius on one side of the cluster centre (‘HALF’; for more details, see de Grijs et al. 2002a). Images with a total exposure time of 1200 s (*V*) and 800 s (*I*) of a nearby field region centred on the LMC’s stellar disc were also used to assess and correct for background contamination (cf. Hu et al. 2010). Figures 1 and 2 show the spatial distributions of the stars associated with the NGC 1805 and NGC 1818 cluster fields, respectively.

Photometry was performed with HSTPHOT (Dolphin 2000), a specialized photometry package for analysis of HST/WFPC2 data sets (for details, see Dolphin 2005; Hu et al. 2010), which can automatically deliver robust HST/WFPC2 photometry as well as the corresponding photometric uncertainties. For each cluster, we obtained point-spread function photometry for the three raw images, which thus resulted in three distinct stellar catalogues. Since bright stars are saturated in the long exposures and faint stars cannot be detected in the short-exposure images, we combined the three catalogues into a complete master data set, retaining only stars with photometric uncertainties up to 0.22 mag. If a given star appeared more than once in our catalogues, we adopted its magnitude and photometric uncer-

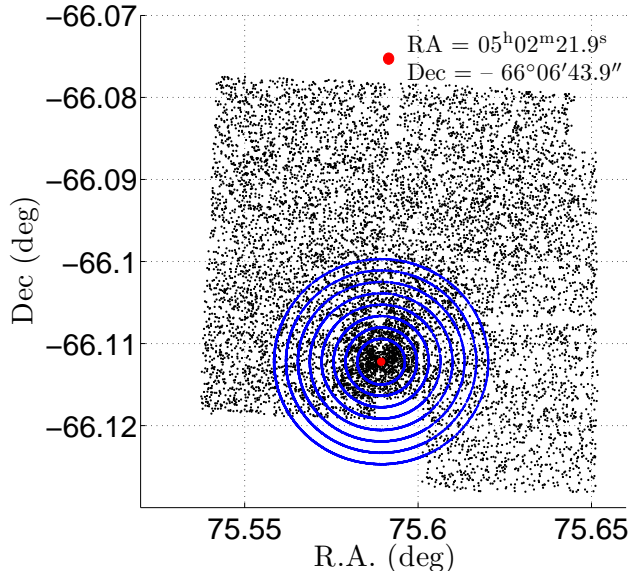


**Figure 1.** Spatial distribution of the stars in the NGC 1805 cluster field. Blue circles are drawn at radii from 10 to 45 arcsec in steps of 5 arcsec. The solid red bullet represents the cluster centre.

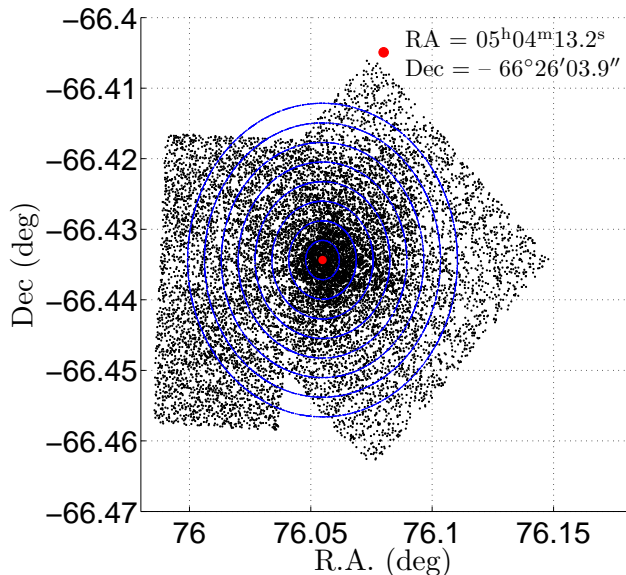


**Figure 2.** As Fig. 1, but for NGC 1818. The blue circles range from 10 to 80 arcsec in steps of 10 arcsec.

tainty based on the deeper observation, which was usually associated with smaller photometric uncertainties. We verified that, in such cases, both entries in our catalogues referred to the same star based on both their magnitudes and spatial coordinates. The spatial distributions of the stars in both cluster fields are shown in Figs 1 and 2.

The photometry of the nearby background field was processed similarly (for details about the background fields, see Castro et al. 2001). We decontaminated the cluster CMDs using a method similar to that employed by Kerber & Santiago (2005) and Hu et al. (2010). We divided

**Table 1.** Stellar numbers in the NGC 1805 and NGC 1818 catalogues.

Name	NGC 1805	NGC 1818
CEN short	1523	2264
CEN long	5785	7189
HALF short	6770	8755
Nearby field	4115	5268
Combined	10770	14067
Decontaminated	6849	9014

both the cluster and field CMDs into a carefully considered number of cells and counted the number of stars in each. For our target clusters, the colour range for both the field and the cluster CMD is approximately 3 mag, while the cluster CMD’s full magnitude range covers more than 10 mag. We divided the cluster and field CMDs into 50 cells in colour and 100 cells in magnitude, with cell sizes of 0.1 and 0.15 mag, respectively. We adopted these cell sizes because of the comparable colour difference between the single-star and binary MSs (see Section 3.2). Small changes in cell size will not affect our decontamination efficiency. However, if we were to define significantly larger cells, this would prevent us from distinguishing substructure in the CMD caused by the binary population, while a significant reduction in cell size would increase stochastic effects and, hence, introduce random-number fluctuations in our background decontamination procedure.

After correcting for the difference in areal coverage, we randomly removed a number of stars corresponding to that in the area-corrected field-star CMD from the cluster CMD. In some bins, the number of field stars was larger than the equivalent number of cluster stars. In such cases, we removed all cluster stars. Although this may lead to increased uncertainties, this situation only occurred near the edges of the relevant area in colour–magnitude space explored; in the region of interest in this paper, covering the genuine single-star and binary MSs, the numbers of cluster stars always exceed those of the field stars. Although the exposure times for the cluster and background CMDs are not identical, here we only investigate the binary properties in a small magnitude range (see below), where both data sets are complete. In Fig. 3 (top row) we display, as an example, the raw CMD of NGC 1805 (left), the CMD of the nearby field region (middle) and the decontaminated CMD (right); for NGC 1818, see fig. 3 of Hu et al. (2010) for an equivalent presentation. We summarize the number of stars in the different raw catalogues and those in the combined catalogues considered for both clusters in Table 1.<sup>1</sup> The panels in the bottom row of Fig. 3 show enlargements of the full CMDs (top row), focussing on the magnitude range of interest for our binarity analysis. In the latter panels, we have also indicated the cell sizes used for our background decontamination.

<sup>1</sup> Since the magnitude range of the background catalogue is not identical to that of the combined catalogue, the decontaminated catalogue contains more stars than the difference between the background and cluster catalogues. For the analysis performed in this paper, we use the decontaminated, combined catalogue.

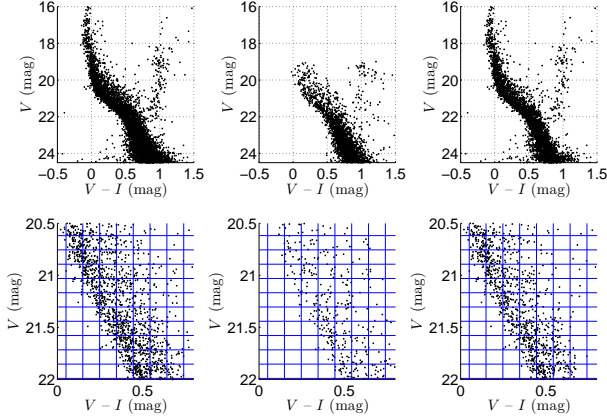


**Figure 3.** (top left) Raw CMD of NGC 1805. (top middle) CMD of the nearby field region. (top right) Decontaminated CMD of NGC 1805. (bottom) Same as the top panels, but highlighting the magnitude range  $V \in [20.5, 22.0]$  mag. We have also delineated the cell sizes used for our background decontamination.

### 3 ISOCHRONE FITTING

#### 3.1 Basic considerations

Distant binaries in crowded environments, such as in compact LMC clusters, cannot be resolved into their individual components with current instrumentation. The fluxes of the individual binary components are thus returned as a single photometric measurement for a given binary system,

$$m_b = -2.5 \log(10^{-0.4m_1} + 10^{-0.4m_2}), \quad (1)$$

where  $m_1$  and  $m_2$  are the magnitudes of the individual components. This means that the binary system will appear as a single object with a brighter magnitude than that of the primary star. Unresolved binaries with MS primary components will thus be biased towards the brighter envelope of the MS.

We used the Bressan et al. (2012) isochrones to describe our decontaminated CMD. Since photometric errors cause the MS to broaden, which hence renders a robust distinction between single stars and low mass-ratio binaries difficult, we determined the photometric uncertainties as a function of magnitude. Following Hu et al. (2010), the relationship is best described by an exponential function of the form  $\sigma(m) = \exp(am+b)+c$ , where  $\sigma$  represents the photometric uncertainty and  $m$  is the corresponding magnitude;  $a$ ,  $b$  and  $c$  are the fit parameters.<sup>2</sup> Figure 4 shows, for NGC 1805, that the functional form of this curve is applicable to our observations (for NGC 1818, see fig. 3 of Hu et al. 2011).

We will now first summarize the fundamental cluster parameters we adopted for our analysis. Based on isochrone fitting, we obtained a distance modulus of  $(m - M)_0 =$

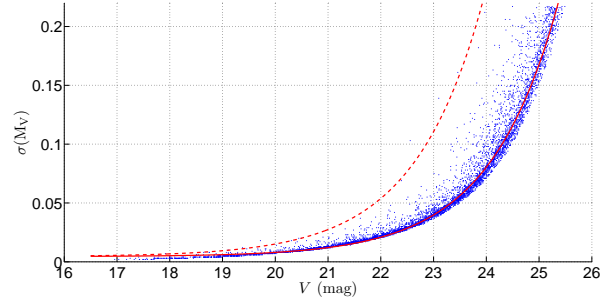


**Figure 4.** Photometric uncertainties as a function of magnitude for the NGC 1805 cluster-centred data set. The red solid line is the best-fitting curve to the distribution’s ridgeline, while the red dashed line represents the  $3\sigma$  range.

$18.50 (18.54) \pm 0.02$  mag for NGC 1805 (NGC 1818). Keeping the distance moduli fixed, we determined ages of  $\log(t/\text{yr}) = 7.65 \pm 0.10$  and  $7.25 \pm 0.10$  for NGC 1805 and NGC 1818, respectively. Our derived age for NGC 1805 is identical to that of Liu et al. (2009b), while the age for NGC 1818 is younger than their estimate  $-\log(t/\text{yr}) = 7.65 \pm 0.05$  – but fully consistent with the age quoted by both de Grijs et al. (2002a),  $\log(t/\text{yr}) = 7.2 \pm 0.1$  and Liu et al. (2009a),  $\log(t/\text{yr}) = 7.25 \pm 0.40$ . We note that because of the young age of NGC 1818, age determination based on isochrone fitting results in significant uncertainties; since Liu et al. (2009b) based their age determination on the faint end of the cluster’s MS, it is likely that their age estimate is an upper limit.

We derive best-fitting extinction values of  $E(B - V) = 0.09 \pm 0.01$  mag for NGC 1805 and  $E(B - V) = 0.07 \pm 0.01$  mag for NGC 1818. The former value is close to the determinations of Santos et al. (2013) and Johnson et al. (2001),  $E(B - V) = 0.075$  mag. Similarly, our extinction estimate for NGC 1818 is consistent with that of both Santos et al. (2013) –  $E(B - V) = 0.07$  mag – and Johnson et al. (2001),  $E(B - V) = 0.075$  mag. We adopted metallicities of  $Z = 0.008$  and  $0.015$  for NGC 1805 and NGC 1818, respectively (cf. Will et al. 1995; Johnson et al. 2001).

For further comparison, Castro et al. (2001) and Liu et al. (2009b) both adopted distance moduli of 18.59 and 18.58 mag for NGC 1805 and NGC 1818, respectively. However, upon close inspection, we note that the isochrones they adopted describe the blue edge of the cluster MSs, while our best-fitting isochrones represent the MS ridgelines. This difference in approach is sufficient to lead to the differences in basic cluster parameters noted here, i.e., our fits yield systematically younger ages and lower extinction values than theirs. We summarize the basic cluster parameters adopted in this paper in Table 2.

#### 3.2 Binary signatures in the CMD

We first adopt the MS ridgeline and the region defined by the  $3\sigma$  photometric errors on either side of the best-fitting single-star isochrone as the area in colour–magnitude space dominated by single stars. Stars brighter and redder than this limit are treated as unresolved binary or multiple systems. Binaries with different mass ratios,  $q = M_s/M_p \leq 1$  (where  $M_p$  and  $M_s$  are the masses of the primary and secondary binary components, respectively), will cause unresolved bi-

<sup>2</sup> These parameters depend only slightly on radius, but the variation of  $\sigma$  over the range from  $V = 20$  to  $V = 22$  mag is very small between the cluster centre and the outer regions. Since the central cluster annuli contain fewer stars than the outer annuli, we checked that using the global uncertainty for the generation of a simulated CMD will not introduce significant differences in our results.

**Table 2.** Basic parameters of NGC 1805 and NGC 1818.

Parameter	NGC 1805	NGC 1818
$\log(t/\text{yr})$	$7.65 \pm 0.10$	$7.25 \pm 0.10$
$Z$	0.008	0.015
$E(B - V)$ (mag)	$0.09 \pm 0.01$	$0.07 \pm 0.01$
$(m - M)_0$ (mag)	$18.50 \pm 0.02$	$18.54 \pm 0.02$
$\alpha_{J2000}$	$05^{\text{h}}02^{\text{m}}21.9^{\text{s}}$	$05^{\text{h}}04^{\text{m}}13.2^{\text{s}}$
$\delta_{J2000}$	$-66^{\circ}06'43.9''$	$-66^{\circ}26'03.9''$
$R_{\text{field}}$ (arcsec)	$45.0 \pm 0.3$	$72.7 \pm 0.3$

aries to attain magnitudes in the ‘binary region’, which are brighter than those defined by the single-star isochrone. We can thus predict where binary systems characterized by different mass ratios are located in colour–magnitude space. For the upper limit of the binary region, we adopt the fiducial binary isochrone for  $q = 1$  (representing equal-mass binaries), i.e., 0.752 mag brighter than the single-star isochrone, plus a  $3\sigma$  photometric uncertainty, where  $\sigma$  is defined by the spread of the bulk of the single-star ridgeline. Figure 3a of de Grijs et al. (2013) shows an example of the resulting single-star and binary regions for NGC 1818.<sup>3</sup> We chose to adopt an upper limit to the binary region to remove some odd objects with extremely red colours. We speculate that these extremely red objects may result from possible triple or higher-order systems. Although this type of stellar system may be rare in regular (open) clusters, triple and higher-order multiple systems may be observable if they are associated with very bright stars in massive clusters.

The multiplicity frequency involving triple and higher-order multiple systems in young massive clusters is unknown. (In the following, when we discuss ‘multiplicity’ we explicitly exclude binary systems from our analysis.) In the solar neighbourhood, Duquennoy & Mayor (1991) found seven triple systems and two quadruples associated with 164 solar-type primary stars, implying a  $5 \pm 2$  per cent multiplicity frequency. Bate (2009) simulated star cluster formation and reported an  $18 \pm 10$  per cent multiplicity frequency for solar-type systems. In addition, in his table 3 the multiplicity frequency seems to increase with increasing primary stellar mass. In this paper, we mainly focus on stars in the range from  $V = 20.5$  (20) to  $V = 22$  (22) mag (see below for justification) for NGC 1805 (NGC 1818), roughly corresponding to F-type stars. Also note that Bate (2009) only simulated initial clouds with a mass of  $500 M_{\odot}$ , while NGC 1805 and NGC 1818 have masses of  $2.8^{+3.0}_{-0.8} \times 10^3 M_{\odot}$  and  $2.3^{+1.1}_{-0.3} \times 10^3 M_{\odot}$ , respectively (de Grijs et al. 2002b).

We hence speculate that these ‘odd’ objects may contain numerous multiple stellar systems, although some may also be caused by occasional multiple blends. Since blending of two (artificial) single stars located along the same line of sight may reach fractions of order 10 per cent in the clusters’ inner regions (see Section 3.4), the probability of triple or higher-order blending is expected to reach fractions of order 1 per cent. However, we add the caveat that possible inadequately decontaminated background stars may also

contribute to their number (for more details regarding the decontamination procedure, see Hu et al. 2010). It is, nevertheless, unlikely that such decontamination artefacts could explain the entire sample of ‘odd’ objects.

Figure 3a of de Grijs et al. (2013) also illustrates why we selected the magnitude range between  $V = 20.5$  and 22 mag for NGC 1805 (and  $V = 20$  to 22 mag for NGC 1818) to explore the properties of the clusters’ binaries. In this region of colour–magnitude space, the effects of binaries are most significant, because the MS slope is shallowest. At brighter magnitudes, the slopes of both the single-star and equal-mass binary isochrones are so steep that they lie very close to one another. In addition, Johnson et al. (2001) suggested that the spread in colour at the brightest extremities of the MSs of both clusters may not only be caused by photometric uncertainties, but that blue straggler stars could also contribute (cf. Li et al. 2013). This hence increases the difficulties associated with investigating binaries at brighter magnitudes in these distant clusters. For stars fainter than  $V \sim 22$  mag, the increasing photometric uncertainties cause a significant broadening of the MS, which causes progressively more binaries to mix with single stars in the CMD, whereas the effects of incompleteness become appreciable ( $\lesssim 50$  per cent completeness) for  $V \gtrsim 24$  mag. In the magnitude ranges probed for our analysis of the clusters’ binary fractions, our sample completeness is well above 80 per cent (de Grijs et al. 2002a, their fig. 2; Hu et al. 2010, their fig. 4; see also Section 3.4).

### 3.3 Cluster centre determination

Since we focus on exploring the binaries’ radial distributions, accurate cluster centre coordinates are essential. We divided the stellar spatial distribution into 20 cells in both right ascension ( $\alpha_{J2000}$ ) and declination ( $\delta_{J2000}$ ). We then proceeded to count the number distributions of stars along both coordinate directions. A Gaussian-like profile was found to provide suitable fits to these distributions; the two-dimensional peak of the adopted Gaussian fits yielded the centre coordinates (see also de Grijs et al. 2013). The resulting coordinates are  $\alpha_{J2000} = 05^{\text{h}}02^{\text{m}}21.9^{\text{s}}$ ,  $\delta_{J2000} = -66^{\circ}06'43.9''$  for NGC 1805 and  $\alpha_{J2000} = 05^{\text{h}}04^{\text{m}}13.2^{\text{s}}$ ,  $\delta_{J2000} = -66^{\circ}26'03.9''$  for NGC 1818.

We next calculated the azimuthally averaged number-density profiles of both clusters (using the full stellar catalogues) and adopted the distances where the clusters’ monotonically decreasing number-density profiles reach the average field level as the clusters’ sizes, i.e.,  $R_{\text{field}} = 45.0 \pm 0.3$  arcsec for NGC 1805 and  $R_{\text{field}} = 72.7 \pm 0.3$  arcsec for NGC 1818 (de Grijs et al. 2013). Mackey & Gilmore (2003) determined radii for NGC 1805 and NGC 1818 of 69 arcsec and 76 arcsec, respectively. Their results are based on surface brightness distributions, so it is reasonable that our results are close but not exactly the same. Figure 5 shows the number-density profiles of NGC 1805 (top) and NGC 1818 (bottom). In Table 2, we have also included information about the cluster sizes and their centre coordinates. At the LMC’s distance, for a canonical distance modulus of  $(m - M)_0 = 18.50$  mag, 1 arcsec corresponds to 0.26 pc.

<sup>3</sup> Note that a precedent exists for this approach: similar approaches were also used by Sollima et al. (2007) and Milone et al. (2012) for Galactic globular clusters.

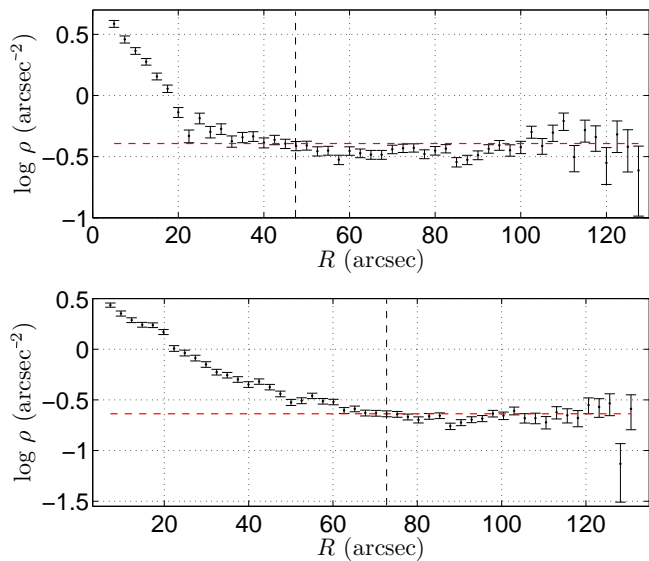


**Figure 5.** Number-density profiles of (top) NGC 1805 and (bottom) NGC 1818. The red dashed lines indicate the field density levels, while the black dashed lines indicate the distances where the clusters’ number densities reach these levels,  $R_{\text{field}}$ .

### 3.4 Artificial-star tests

An important effect contributing to broadening of the MS is blending of otherwise unrelated stars due to crowding and line-of-sight projection. This causes a similar observational signature as that owing to the presence of binary systems. To avoid possible overestimates of the binary fraction caused by stellar blends, we estimated the blending ratio at different radii using artificial-star (AS) tests. We adopted the approach of Hu et al. (2010), which was optimized for application to observations obtained with the *HST*/WFPC2 camera, specifically to our observations of NGC 1818. Based on blending experiments of ASs of different luminosities, they found that two objects which are separated by fewer than 2 pixels cannot be resolved. We adopted their approach to obtain the blending fractions at different radii, taking into account that

- (i) stars may blend with each other along the line of sight, especially in very crowded environments; and
- (ii) stellar positions may be coincident with those of cosmic rays or extended objects, which may prevent their robust detection.

In general, a large fraction of the brightest objects in our database are predominantly caused by blending. Since our data set of interest in this paper is based on a selection that is significantly brighter than the detection limit, following Hu et al. (2010) we added more than 640,000 ASs to the observed, decontaminated stellar catalogues, and subsequently compared their positions to those of all observed objects (including stars and extended objects, although we removed possible cosmic rays from the raw images; this is a negligible effect). Stars which are blended with extended sources will be detected as extended sources and removed from the sample; only stars that actually blend with other

stars will produce a ‘blending binary’, which will cause a systematic offset of the binary fractions’ radial profiles.

We imposed that the ASs obey a luminosity function (LF) corresponding to a Salpeter-like stellar mass function and that their magnitude and colour distributions follow the best-fitting isochrones. We then examined every single AS to check whether it would blend with any observed object. To do so, we adopted a minimum distance of 2 pixels between artificial and observed stars as the blending criterion (cf. Hu et al. 2011, their figs 4–8). If this criterion was met, we assumed that the fainter of the two objects would be dominated by its brighter counterpart. We then calculated the ratio of the number of blended objects (‘optical pairs’) to the total number of stars in our sample,  $f_{\text{opt}} = N_{\text{blend}}/N_{\text{tot}}$ , where  $N_{\text{blend}}$  and  $N_{\text{tot}}$  represent the number of relevant objects within a given magnitude range, and  $f_{\text{opt}}$  is a function of magnitude. Figure 6 shows the blending fraction for NGC 1805 as a function of clustercentric radius and magnitude.

For faint stars, we also need to consider the detection limit. The observed LF sharply decreases at a given magnitude because of the onset of sampling incompleteness. In this case, not only stellar blends affect the detection limit, but a fraction of the fainter stars may also remain hidden below the detection level. In addition, the combination of these effects with the complicated structure of the stellar LF will affect the final shape of the radius-dependent completeness curve.

To determine our data sets’ completeness curves, we generated ASs, which we first added to the reduced science images and subsequently recovered using the same photometric approach as employed to obtain our main stellar databases (cf. Baily et al. 1992; Rubenstein & Baylin 1997, among many others). We used *HST*PHOT to generate ASs covering the magnitude range  $V \in [19, 26]$  mag and  $(V - I)$  colours from 0.0 to 1.8 mag, roughly following the distribution of the observational CMD based on the medium exposure-time images. Note that this fully covers the magnitude range of interest here,  $V \in [20.0, 22.0]$  mag, which we discuss in detail below.

Because of the crowded environments of NGC 1805 and NGC 1818, we would need to generate more than  $10^5$  ASs per image to obtain statistically robust completeness estimates. However, to avoid blends between ASs and significant increases of the background’s brightness level, in practice we only added several tens of ASs to our images. In total, we generated roughly 160,000 ASs for our analysis of both the NGC 1818 and NGC 1805 *HST* fields, using 70 to 80 stars at a time. All ASs were randomly distributed across the chips, a process we repeated 4000 times to reduce statistical fluctuations. Figure 7 displays the 3D ‘completeness plane’ thus obtained. Since both single stars and binary systems are point sources at the distance of the LMC, our observations’ completeness fractions are simple functions of radius and magnitude. We thus applied completeness corrections in the standard manner using the 3D completeness plane of Fig. 7.

In the Appendix, we compare the completeness curves based on both simulated AS tests (Hu et al. 2011) and real AS tests (this paper). Hu et al. (2011) reported that their approach can reproduce the completeness curve for their set of *HST* images. However, we found that this may only fully apply to sparsely covered images, such as that represented

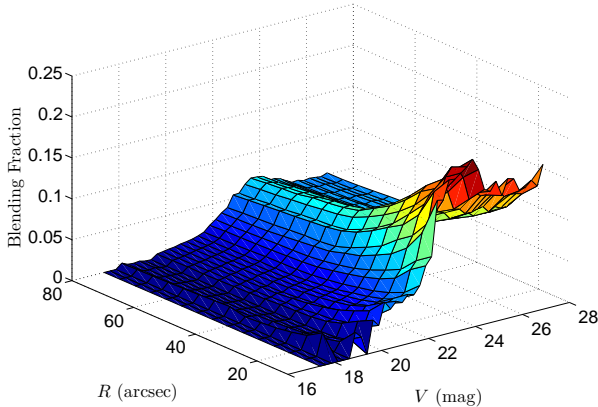


**Figure 6.** Blending fraction as a function of radius and magnitude for NGC 1805.

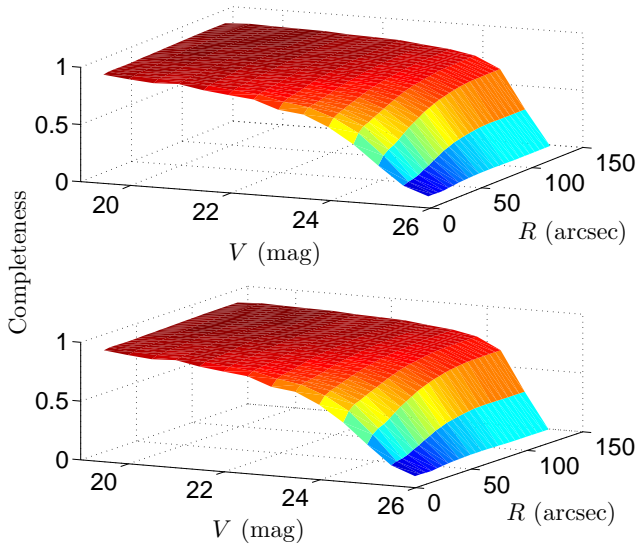


**Figure 7.** Sample completeness as a function of radius and magnitude for (top) NGC 1805 and (bottom) NGC 1818.

by the WF3 chip of our NGC 1818 observations (Hu et al. 2011). In significantly more crowded environments, saturated stars will introduce significant levels of incompleteness which must be duly taken into account.

We next calculated the number of stars located in the single-star region in the CMD divided by that found in the ‘binary region’, corrected for the corresponding blending fraction of optical pairs,  $f_{\text{opt}}$ , at different radii for all stars in the magnitude range of interest for our binarity analysis,

$$f_{\text{bin}} = \frac{N_{\text{b}}}{(N_{\text{b}} + N_{\text{s}})} - f_{\text{opt}}, \quad (2)$$

where  $N_{\text{b}}$  and  $N_{\text{s}}$  represent the numbers of stars located in the ‘binary’ and ‘single-star regions’, respectively. We calculated the resulting ‘cumulative binary fractions’,  $f_{\text{bin}}$ , for radii from  $R \leq 10$  to  $R \leq 45$  arcsec ( $R \leq 10$  to  $R \leq 80$  arcsec) in steps of 5 (10) arcsec for NGC 1805 (NGC 1818) and adopted Poissonian uncertainties. Since the number of

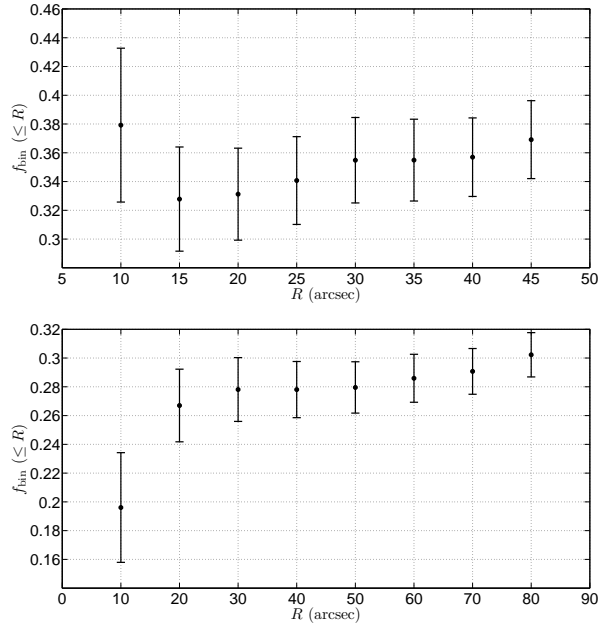


**Figure 8.** Cumulative binary fraction radial profiles of (top) NGC 1805 and (bottom) NGC 1818. Error bars represent Poissonian uncertainties.

stars decreases as the radius decreases, for  $R < 10$  arcsec the number of objects is not statistically significant.

Figure 8 shows the (cumulative) binary fractions’ radial profiles for NGC 1805 and NGC 1818. In the inner regions of both clusters, opposite trends can be seen. In NGC 1805, the binary fraction first strongly decreases with increasing radius in the central region, followed by a slightly and monotonically increasing trend to the cluster’s outskirts, until it reaches the level of the field’s binary fraction. Meanwhile, NGC 1818 displays a monotonically increasing trend with radius, especially in the innermost regions (cf. de Grijs et al. 2013). We will discuss the significance of these results in Section 5.2.

#### 4 $\chi^2$ MINIMIZATION

We used a more sophisticated and physically better justified approach, based on Monte Carlo simulations and  $\chi^2$  minimization, to test whether the isochrone-fitting results obtained in the previous section are robust. Using the best-fitting isochrones, for each WFPC2 chip we can now simulate a stellar catalogue representing a CMD that is similar to that of the observed sample. Our AS tests were used to create millions of ASs. For each chip, we randomly distributed these across an  $800 \times 800$ -pixel coordinate system. The ASs were drawn from a Salpeter-like mass function, and the corresponding magnitudes in both the  $V$  and  $I$  filters were obtained from interpolation of the isochrones. Gaussian noise was added to all stars according to the best-fitting relation based on Fig. 4.

We next transferred the  $(x, y)$  pixel coordinates for all stars to the corresponding  $(\alpha_{\text{J2000}}, \delta_{\text{J2000}})$  values. For each observed star, we first selected the nearest 20 ASs as possible counterparts. If the observed object was brighter than

$V = 20$  mag, even if it were an unresolved binary, it would likely mix with the genuine single stellar population because of the steepness of the CMD: Fig. 9 shows the theoretical ridgelines of single stars and of unresolved binary systems characterized by different mass ratios. Unresolved binaries fainter than  $V = 23$  mag can also not be distinguished because of the photometric uncertainties affecting our data. For such stars, we adopted the AS characterized by the most similar magnitude and colour as representative counterpart of the observed star of interest. For observed stars with magnitudes between  $V = 20$  and  $V = 23$  mag, we first determined their relative positions with respect to the  $q = 0.6$  binary population’s ridgeline. (In our analysis below, we will use a minimum mass-ratio cut-off of  $q = 0.55$ . In view of the uncertainties in  $q$ , here we conservatively choose  $q = 0.6$  as the minimum mass ratio.) If an observed star is bluer than this locus, we again choose the AS with the most similar magnitude and colour as its best-matching counterpart. If it is located on the red side of the  $q = 0.6$  boundary but characterized by a colour that is bluer than that of the  $q = 0.8$  locus, we first calculate the primary star’s magnitude under the assumption that the observed object is either a  $q = 0.6$  or a  $q = 0.8$  binary. We then adopt the average magnitude instead of that of the observed object and find the AS with the most similar magnitude to that inferred for this primary star. Since all ASs are single stars, the ASs that most closely match our observed data points hence automatically attain the proper colours for these primary stars, *modulo* the photometric uncertainties. For observed stars that are located between the  $q = 0.8$  and  $q = 1.0$  binary loci, we apply a fully equivalent procedure. Stars that are located beyond the red side of the  $q = 1.0$  binary locus are all treated as equal-mass binaries, so that we simply add 0.752 mag to both their  $V$  and  $I$  magnitudes. The resulting stars are hence the primary stars of the binary systems that may be contained in our photometric database. Figure 10 displays the differences between the observed stars and the associated primary stars if we assume the observed photometric data points to reflect the colours and magnitudes of binary systems. The different colours indicate different mass ratios, specifically for  $q = 0.6, 0.8$  and  $1.0$ .

We thus generated a simulated cluster with an identical number of stars, a similar spatial distribution to the observed cluster and a similar CMD compared with that composed of the observed single stars and primary stars of the unresolved binary systems. Again, we use NGC 1805 as an example to show the comparison between the simulated and observed clusters. Figure 11 (top) shows the CMD of our simulated cluster, without inclusion of any binaries or optical pairs but instead composed of the binary system’s primary stars, and that of the single-star regime pertaining to NGC 1805. Figure 12 shows the corresponding spatial distributions. The remaining free parameters which will cause the distribution of the CMD of the simulated cluster to differ from the observed CMD are the relevant mass-ratio distribution of the clusters’ binary components and the binary fraction.

The binary mass-ratio distribution we need to adopt for our simulations is not set arbitrarily. For binaries in massive clusters, the most appropriate mass-ratio spectrum is still unknown, however. Hu et al. (2010) chose a flat spectrum (i.e., characterized by a power-law index,  $\alpha = 0$ ) for NGC

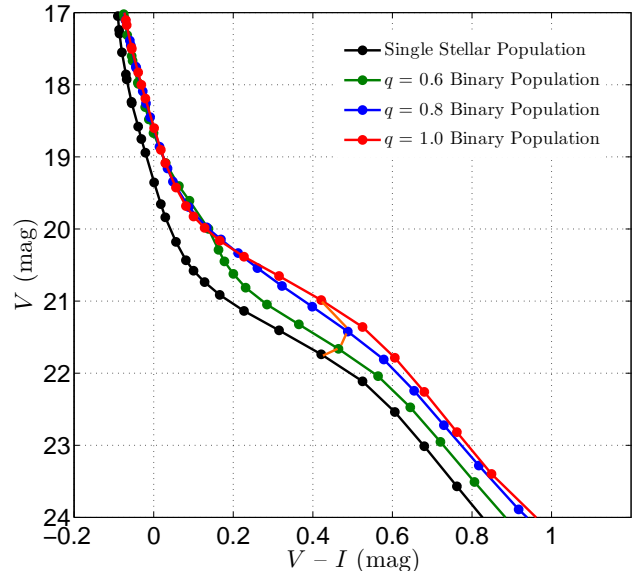


**Figure 9.** Ridge lines for NGC 1805 of single and binary stellar populations characterized by different mass ratios, based on the Bressan et al. (2012) isochrones.

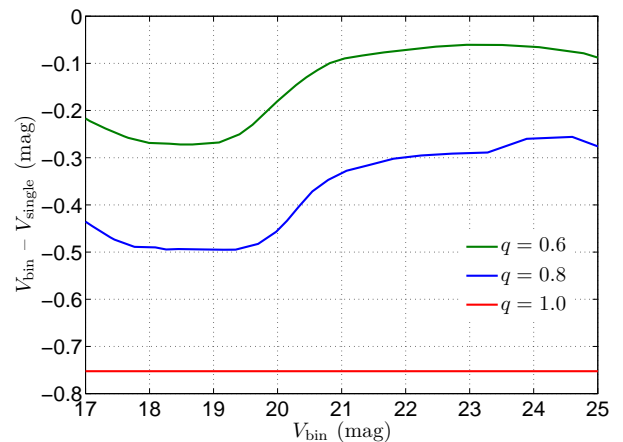


**Figure 10.** Magnitude differences between binaries and their single-star primaries. Green, blue and red lines represent mass ratios of 0.6, 0.8 and 1.0, respectively.

1818, while Kouwenhoven et al. (2005, 2007) found that a power-law spectrum with an index of  $\alpha = 0.4$  (i.e., low mass-ratio dominated) appears suitable for binaries in low-density environments. Reggiani & Meyer (2011) also suggested a typical range of  $\alpha \in [0.0, 0.4]$ . In fig. 3c of de Grijs et al. (2013), we showed that if we adopt a proper mass ratio cut-off (here we initially use  $q \geq 0.55$ , see below) to mimic the uncertainties caused by contamination of the binary region by single stars, the value of the resulting binary fraction does not significantly depend on  $\alpha$  (see below for further improvements). Therefore, we adopted fixed power-law spectra for the binary mass-ratio distribution with indices of  $\alpha = 0$  and  $0.4$  for our tests (see below). In general, the free input



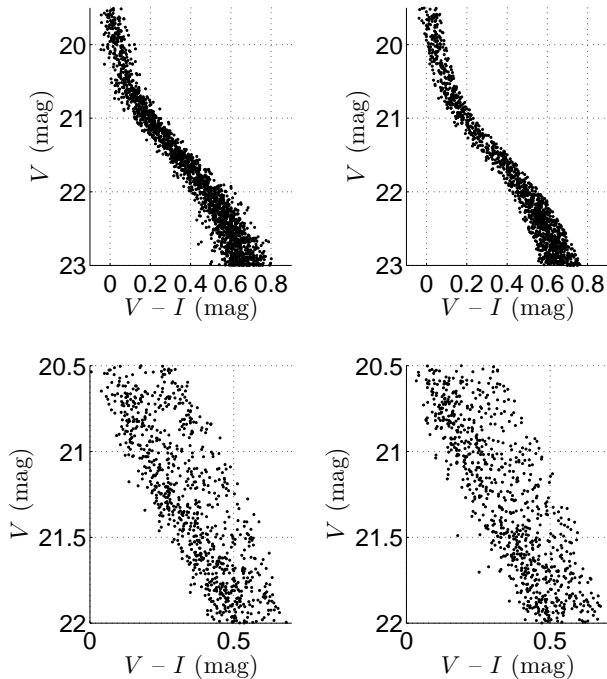


**Figure 11.** (top left) CMD of the simulated cluster, not including any binaries. (top right) Observed CMD of NGC 1805 (‘single stars’ only, i.e., data points found within  $\pm 3\sigma$  of the MS ridgeline). (bottom left) Simulated cluster CMD, characterized by 40 per cent binaries and a flat mass-ratio distribution. (bottom right) CMD of NGC 1805.

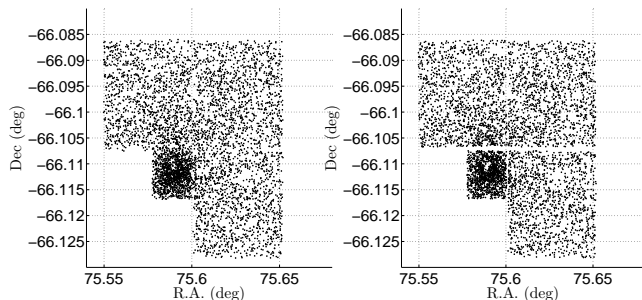


**Figure 12.** Spatial distributions of (left) our simulated cluster and (right) NGC 1805.

parameters are, therefore, the power-law index,  $\alpha$ , and the binary fraction,  $f_{\text{bin}}$ .

For our analysis of NGC 1805 (NGC 1818), we added artificial binaries with binary fractions ranging from 5 to 90 per cent, in steps of 5 per cent, to the selection of observed stars. However, because of photometric uncertainties, binaries with  $q \leq 0.55$  are largely mixed with the single stars. We thus first adopted a lower mass-ratio cut-off of  $q = 0.55$  for our analysis (but see below); these binaries will appreciably broaden the MS of the simulated CMD towards brighter (and redder) photometric measurements. All stellar photometry (including binaries) follows the empirical uncertainties (see Fig. 4). Figure 11 (bottom) shows an example of a sim-

ulated CMD (characterized by 40 per cent binaries and a flat-mass ratio spectrum) and the observed CMD of NGC 1805. Our simulations are not directly corrected for the effects of incompleteness: because we determined the incompleteness levels independently and separately, we corrected the simulations for these effects upon their completion.

We again adopt the same fiducial line as used for our isochrone-fitting approach to divide the simulated CMD into single-star and binary regions. For different input binary fractions, we count how many ASs are located in the single-star region,  $N_{\text{s}}$ . These may not all be single stars, because some binaries characterized by low mass ratios may also be located in this region. We also count how many ASs are located in the binary region,  $N_{\text{b}}$ . These stars may not all be binaries either, since this sample may also contain single stars characterized by a large colour spread. We take one simulation result of NGC 1805 as an example, assuming a flat mass-ratio spectrum. The best-fitting model for  $R \leq 45$  arcsec contains 280 single stars and 125 binaries with  $q \geq 0.55$ , i.e.,  $f_{\text{bin}} = 30.9$  per cent. Further exploration shows that among these 125 binaries, 12 are located in the single-star region, while 16 single stars in the simulation have scattered into the binary region. Our simple isochrone-fitting method would result in  $f_{\text{bin}} = 31.9$  per cent. The mixture of binaries and single stars hence results in an overestimation of approximately one per cent based on the isochrone-fitting approach applied to this cluster. Similarly, if we adopt a power-law mass-ratio spectrum with an index of 0.4 ( $\alpha = 0.4$ ), the mixture will cause an underestimation of 1.4 per cent. (The number of single stars with a large colour spread remains, but more low mass-ratio binaries will scatter into the single-star region.) The larger  $\alpha$  is, the higher the number of low mass-ratio binaries becomes, which hence leads to a larger underestimation, i.e.,  $f_{\text{bin(iso)}}$  remains constant but  $f_{\text{bin}(\chi^2)}$  increases. The equivalent *observed* stellar numbers derived from our isochrone-fitting approach are denoted  $N'_{\text{s}}$  (all treated as single stars) and  $N'_{\text{b}}$  (all treated as binaries). We then perform  $\chi^2$  minimization:

$$\chi^2 = \left( \frac{N'_{\text{s}} - N_{\text{s}}}{\sigma_{N_{\text{s}}}} \right)^2 + \left( \frac{N'_{\text{b}} - N_{\text{b}}}{\sigma_{N_{\text{b}}}} \right)^2, \quad (3)$$

where  $\sigma_{N_{\text{s}}}$  and  $\sigma_{N_{\text{b}}}$  are the statistical (Poissonian) errors associated with the numbers of ASs, so that

$$\chi^2 = \frac{(N'_{\text{s}} - N_{\text{s}})^2}{N_{\text{s}}} + \frac{(N'_{\text{b}} - N_{\text{b}})^2}{N_{\text{b}}}. \quad (4)$$

The  $\chi^2$  value indicates the level of similarity between the simulated and observed CMDs. We vary  $f_{\text{bin}}$  from 5 to 90 per cent and determine the minimum  $\chi^2$  value for each input binary fraction. Our aim is to determine the global minimum  $\chi^2$  value. We therefore use a quadratic function to fit the  $\chi^2(f_{\text{bin}})$  distribution, which will give us both the global minimum  $\chi^2$  value (and, hence, the best-fitting binary fraction) and its  $1\sigma$  uncertainty (see also de Grijs et al. 2013). The latter corresponds to the difference between  $\chi^2_{\text{min}}$  and  $\chi^2_{\text{min}} + 1$  (Avni 1976; Wall 1996). Figure 13 provides an example of a typical  $\chi^2(f_{\text{bin}})$  distribution and its corresponding  $1\sigma$  uncertainty. For each radius, we derive  $\chi^2_R(f_{\text{bin}})$  using 10 independent generalizations to minimize fluctuations caused by random scatter. Figure 14 shows the resulting average  $\chi^2_R(f_{\text{bin}})$  for NGC 1818 for radii from  $R \leq 10$  to  $R \leq 80$  arcsec in cumulative steps of 10 arcsec. Once we have ob-

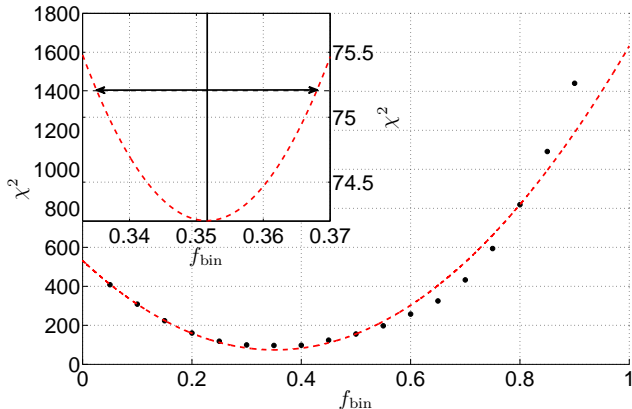


**Figure 13.** Typical  $\chi^2(f_{\text{bin}})$  distribution. The red dashed line is the best-fitting quadratic curve, the double arrow in the inset indicates the  $1\sigma$  uncertainty and the vertical black line indicates the best-fitting  $f_{\text{bin}}$ .

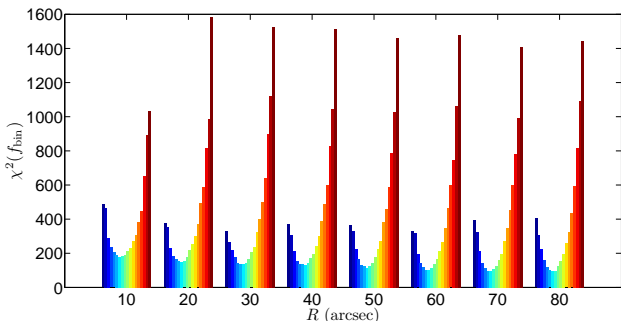


**Figure 14.** Distribution of  $\chi^2_R(f_{\text{bin}})$  for NGC 1818, from  $R \leq 10$  to  $R \leq 80$  arcsec. The colour scale represents  $f_{\text{bin}}$ , from 5 to 90 per cent.

tained the best-fitting binary fraction from Fig. 14, we correct for blending using the results from Fig. 6 (see also the Appendix).

The  $f_{\text{bin}}(\leq R)$  distribution following deblending hence represents the cumulative binary fraction’s radial profile based on  $\chi^2$  minimization. We display the results of the  $\chi^2$  tests for NGC 1805 and NGC 1818 in Fig. 15, where the top and bottom panels represent NGC 1805 and NGC 1818, respectively (blue and red dashed lines for mass-ratio distributions assuming, respectively,  $\alpha = 0.0$  and  $0.4$ ). We also compare the results of our  $\chi^2$  minimization with the isochrone-fitting approach (black dashed line) in the same figure. The comparison shows that both methods mutually agree very well, which hence implies that both the general behaviour and the actual levels of the radial profiles of the clusters’ cumulative binary fractions derived here are robust.

Our imposition of a mass-ratio cut-off at  $q = 0.55$  is not strictly necessary to reach convergence. We merely adopted this limit because we wanted to properly compare the results from both methods. We will now release this restriction, although in this case we need to make an informed assumption about the mass-ratio distribution at low mass ratios. For simplicity and based on the scant observational evidence at hand (see above), we assume that for all  $q$  the

mass-ratio distribution is adequately represented by a flat spectrum, i.e.,  $\alpha = 0.0$ . As expected, the result, which is also included in Fig. 15 (solid blue lines), shows a clearly higher binary fraction compared to our results for  $q \geq 0.55$ . However,  $\chi^2$  minimization results in the same trend of binary fraction versus radius as found from our isochrone fits. In fact, this also shows that the isochrone-fitting approach can only be used to derive what has been called a ‘minimum binary fraction’ (cf. Sollima et al. 2007; Milone et al. 2012).

Let us now compare the actual binary fraction determined here with those resulting from previous work for representative stellar systems. First, Sollima et al. (2010) analysed the binary fractions in five Galactic open clusters using a similar approach as that adopted in this paper. Adoption of mass-ratio cut-offs of  $q \geq 0.48$  to  $q \geq 0.55$  leads to core binary fractions between 11.9 and 34.1 per cent in their five sample clusters. They also estimate a ‘complete’ binary fraction, i.e., without imposing a mass-ratio cut-off, and find binary fractions between 35.9 and 70.2 per cent. Clearly, the binary fraction of NGC 1818 falls within their range of values if we adopt a core radius of roughly 10 arcsec (see Mackey & Gilmore 2003, their table 4). We expect that the core binary fraction of NGC 1805 should be significantly higher than any of the values reported by Sollima et al. (2010): Mackey & Gilmore (2003) derive a cluster core radius for NGC 1805 of  $5.47 \pm 0.23$  arcsec, whereas we only explored the binary fraction for radii in excess of 10 arcsec because of the statistically small number of stars in the cluster core.

Second, Milone et al. (2012) derived the (core) binary fraction of 59 Galactic globular clusters. Their resulting values are significantly smaller than the values we derive for the young massive clusters NGC 1805 and NGC 1818. They find a maximum core binary fraction of only roughly 17 per cent, for a mass-ratio cut-off of  $q = 0.5$ . The fact that our results yield systematically higher binary fractions than those reported previously for both globular and open clusters is not a surprise, not even for the open clusters. In old globular clusters, the cluster cores will have undergone billions of years of dynamical processing (this also applies to the intermediate-age open clusters of Sollima et al. 2010), while the binaries in our two young sample clusters are still in the early stages of their stellar and dynamical evolution. We will return to the evolution of binary systems in dense star clusters and the relevant time-scales involved in Section 5.3.1.

We also checked whether the resulting binary fractions depend on  $\alpha$ . We found that the choice of  $\alpha$  (within observational limits) does not affect the main trend of the binary fractions’ radial profiles, but it instead determines the relative slope and the value of the binary fraction at a given radius. This is expected, since a steeper mass-ratio distribution (larger  $q$ ) produces more low mass-ratio binaries, which will be indistinguishable from single stars. In Figs 16 and 17, the 3D surface figures display the derived binary fraction as a function of both  $\alpha$  and radius,  $f_{\text{bin}}(\alpha, \leq R)$ . For both clusters, the main trend appears stable and robust for  $\alpha \leq 0.5$ . This hence shows that our choice of  $\alpha \in [0.0, 0.4]$  is reasonable.

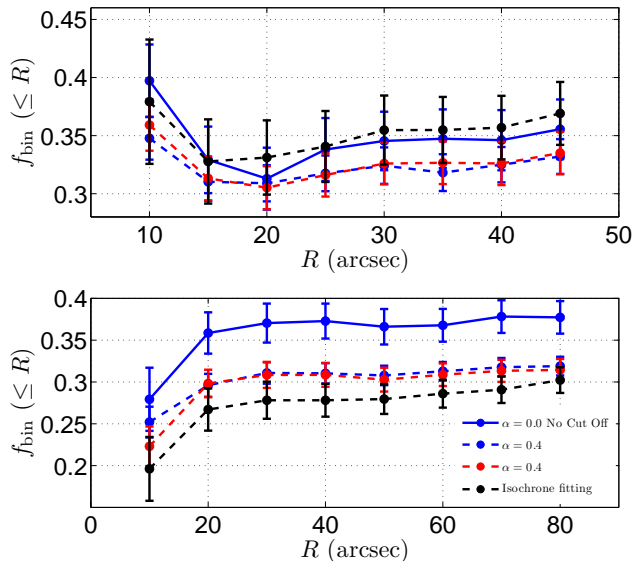


**Figure 15.** Cumulative binary fraction radial profiles of (top) NGC 1805 and (bottom) NGC 1818 obtained on the basis of both our  $\chi^2$  tests and isochrone fitting. The blue and red dashed lines represent the results from our  $\chi^2$  minimization for flat and power-law mass-ratio spectra with a  $q \geq 0.55$  cut-off ( $\alpha = 0.0$  and 0.4), respectively; the blue solid lines are for  $\alpha = 0.0$  and no mass-ratio cut-off. The black dashed lines indicate the results from our isochrone fits.

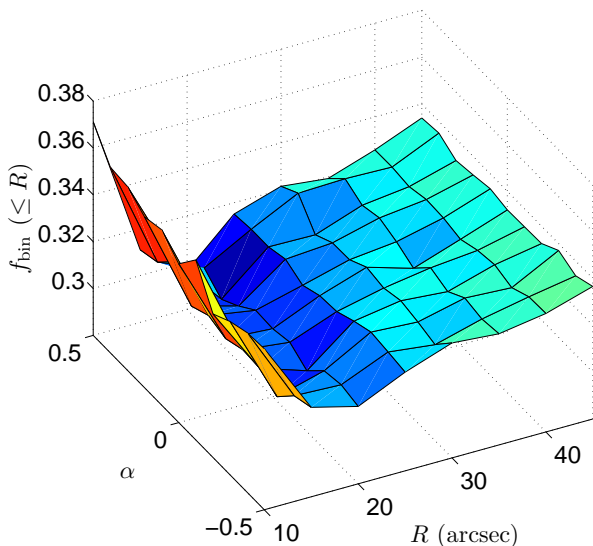


**Figure 16.** 3D surface of  $f_{\text{bin}}(\alpha, R)$  for NGC 1805.

## 5 DISCUSSION

### 5.1 Improvement of previous work

Following publication of de Grijs et al. (2013), we significantly improved the code we developed for  $\chi^2$  minimization, which in turn enables us to obtain more accurate results which are affected by smaller uncertainties. Our main im-

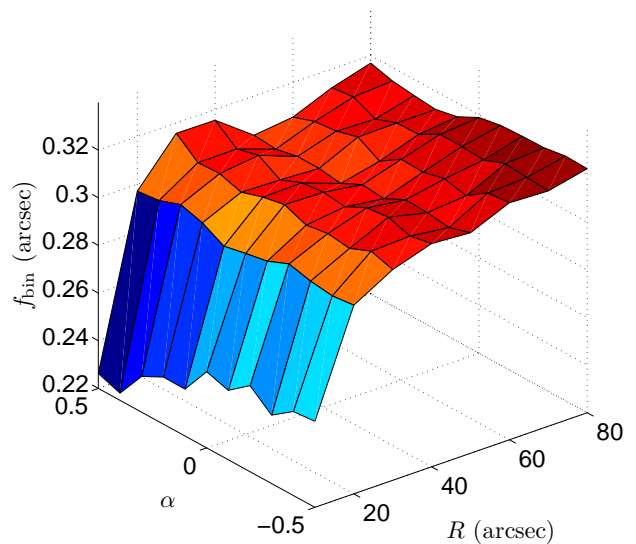


**Figure 17.** As Fig. 14, but for NGC 1818.

provement is related to the way in which we divide the CMD into cells to calculate  $\chi^2(f_{\text{bin}})$ . In de Grijs et al. (2013), we used six cells to cover the colour difference,  $\Delta(V-I)$ , adopting best-fitting isochrones as the colour zero points (hereafter ‘pseudo-colours’). We also used three cells in the magnitude direction. However, we found that dividing the CMD in this manner is not necessary. First, adoption of three cells in magnitude cannot distinguish any differences between the simulated model and the observed cluster; the cells in the magnitude direction are only sensitive to the difference between the adopted and the real LFs. Since we adopted a fixed LF for our simulated cluster, the cells in magnitude will contribute nothing but a constant  $\chi^2$ , and hence increase the uncertainty.

It also transpired that selection of six cells along the pseudo-colour axis represented too much subdivision. Since we adopted  $q \geq 0.55$  for all binaries, the three bluest cells cannot be used for distinction of any binaries either. The maximum uncertainty in the binary fraction reported in de Grijs et al. (2013) reached 9.9 per cent, with an average uncertainty of 4.4 per cent. For this reason, we needed to rely on Student’s  $t$ -test scores to estimate at which level our results were statistically significant. Because of the sizeable uncertainties, the results from our isochrone-fitting approach could only be used as additional support.

In this paper, we mimicked the cell-division method applied to our isochrone fits to proceed with our  $\chi^2$ -minimization test. In this case, the results from our isochrone fits can be used both in support of our conclusion based on the  $\chi^2$ -minimization approach and as a comparison method of similar accuracy. Ignoring any uncertainties that may have been caused by our assumptions of a constant LF and of the shape of the mass-ratio spectrum at different radii (see Section 5.2 for a discussion), the shape of  $f_{\text{bin}}(\leq R)$  resulting from  $\chi^2$  minimization should be very similar to that based on our isochrone fitting.

Compared with de Grijs et al. (2013), the most impor-

tant improvement we present here is the significantly improved (i.e., reduced) level of uncertainty. For instance, for NGC 1818 and assuming  $\alpha = 0.0$  (0.4), the average uncertainty in the binary fraction is only 1.3 (1.6) per cent. This is significantly smaller than that presented in our previous work, to the extent that the radial increase of the binary fraction in NGC 1818 is now clearly statistically robust and we no longer need to rely on complex statistical tools to assess the level of significance.

## 5.2 Comparison of the approaches

The isochrone-fitting method is independent of any assumptions as regards the detailed physical parameters such as the shape of the stellar mass function and the binary components' mass-ratio distribution. In addition, NGC 1805 and NGC 1818 are sufficiently young that we do not need to consider possible contamination from multiple stellar populations. Introduction of multiple stellar populations becomes important only for intermediate-age massive star clusters, many of which exhibit a significant double or extended MS turnoff (Mackey & Broby 2007; Mackey et al. 2008; Girardi et al. 2009; Milone et al. 2009).

Some authors have suggested that double or extended MS turnoffs in intermediate-age massive clusters may be owing to rapid stellar rotation (e.g., Bastian & de Mink 2009; Li et al. 2012), because the resulting centrifugal support will decrease the effective temperatures and luminosities of the stars. This fast-rotation effect may not only affect intermediate-age but also young massive clusters. To estimate the possible effect of fast rotation in the context of our target clusters, we follow Bastian & de Mink (2009) and adopt a rotation rate of  $\omega = 0.55$  (expressed as fraction of the critical break-up rotation rate) and a standard deviation of 0.15. We also assume that  $\omega$  increases linearly with mass from  $1.2 M_{\odot}$  to  $1.5 M_{\odot}$  (cf. Li et al. 2012). In intermediate-age massive clusters, the reddening caused by rapid rotation is quite significant for stellar masses close to  $1.5 M_{\odot}$  (corresponding to apparent magnitudes at the distance of the LMC near  $V = 20$  mag). On the other hand, for our target clusters this effect is trivial, because at intermediate ages such stars are found near the MS turnoff while in young massive clusters they are still located on or very near the zero-age MS and attain very blue (hot) colours. The temperature decrease caused by rapid rotation is insignificant compared with the temperature of non-rotating stars.

Taking NGC 1805 as an example, Fig. 18 shows the best-fitting isochrones for no and fast rotation. The two ridgelines are quite close, characterized by an offset of only approximately 0.02 mag in colour. We therefore added 0.02 mag to the photometric uncertainties of our sample stars in the relevant magnitude range. The minimum age for which a distinct effect of rotation on the MS locus of massive clusters would show up is still unclear. Yang et al. (2013) suggest that, at least for massive clusters younger than 0.6 Gyr, the effects of rotation are insignificant.

More importantly, however, isochrone fitting is limited by the necessity to impose a minimum binary fraction in our analysis. Because the intrinsic colour spread of single stars caused by photometric uncertainties broadens the MS, only stars that are found significantly beyond the MS in colour–magnitude space can be treated robustly as binaries.

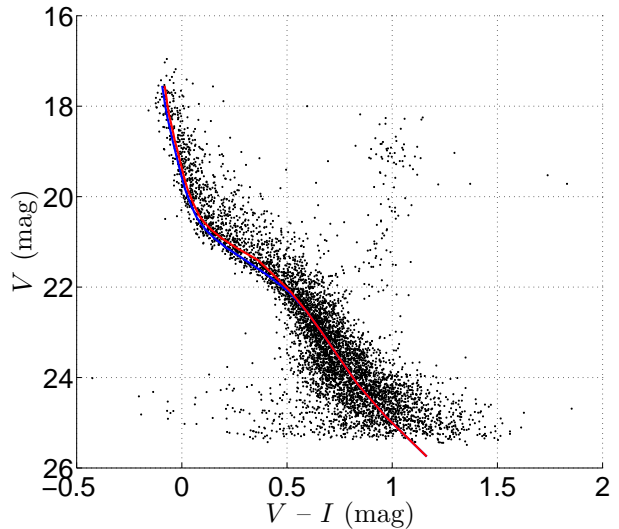


**Figure 18.** Effect of rapid stellar rotation in NGC 1805. The blue line represents the best-fitting isochrone without considering rapid rotation; the red line is for rapidly rotating stars ( $\omega = 0.55$  of the critical break-up rotation rate). Only a small offset is seen for  $V \in [20, 22]$  mag.

In addition, Poissonian uncertainties will further reduce the number of useful objects in the innermost regions of dense clusters.

Alternatively, our newly developed  $\chi^2$  minimization approach can, in principle, be used to determine binary fractions more accurately and for a larger range of mass ratios. In the context of isochrone fitting, the uncertainties are driven by the total number of stars, so that the absolute errors increase with decreasing radii. For instance, for NGC 1805, isochrone fitting (assuming a flat mass-ratio distribution) yields uncertainties that increase from 2.5 to 5.4 per cent as radii decrease from 45 arcsec to 10 arcsec. However, the uncertainties associated with our  $\chi^2$  minimization increase only from 1.5 to 1.8 per cent for the same radial range (a power-law mass-ratio distribution also returns uncertainties of better than 2 per cent), because the absolute uncertainties only depend on the slope of  $\chi^2(f_{\text{bin}})$  as a function of radius (cf. Fig. 14).

However, the main disadvantage of our  $\chi^2$ -minimization approach is that it takes a relatively large amount of computer time compared to isochrone fitting. For example, for each of our tests we ran simulations using roughly 2 million ASs. A single simulation takes approximately 3 min in a normal core i7 CPU environment. For each cluster, we ran the simulations 10 times in eight radial bins to determine the average  $\chi^2(f_{\text{bin}})$  distribution for a given radial range. This hence consumes around 4 hr. Our tests in which we varied the mass-ratio distribution from  $\alpha = -0.9$  to  $+0.9$  in steps of  $\Delta\alpha = 0.1$  showed that the total computer time required for one cluster was  $4 \times 19 = 76$  hr. Using standard multiple processors, these tests would still take of order 2 days to complete.

In addition, for the  $\chi^2$  tests, we need to assume a mass function and a mass-ratio spectrum for the binary population. However, the mass function is likely to vary as a function of radius because of the effects of mass segregation. At

the same time, binaries characterized by low mass ratios in the clusters' inner regions will be preferentially disrupted, so that the mass-ratio distribution will also vary as a function of radius. For instance, from Fig. 14 it is clear that even though the  $\chi^2(f_{\text{bin}})$  distributions at different radii are all quite smooth, the distribution for  $R \leq 10$  arcsec is systematically and significantly offset to higher mass ratios compared with the other radii. This means that the assumption of a uniform mass function and a constant mass-ratio spectrum for the entire cluster is inappropriate. However, since the shape of the binary fraction's radial profile does not vary very significantly, we nevertheless adopted a simple, single mass function and mass-ratio distribution to limit the total amount of computing time needed for our simulations.

### 5.3 Physical implications

#### 5.3.1 Binary segregation

The cumulative binary fraction's radial profile in NGC 1805 displays a significant decreasing trend for the innermost two radial bins ( $R \leq 15$  arcsec), followed by a slight increase to the field's binary fraction. Since binaries are, on average, more massive than single stars of similar spectral types, it is reasonable to conclude that mass segregation is likely responsible for the behaviour of the radial binary fraction in NGC 1805.

de Grijs et al. (2002b) reported a clear detection of the effects of mass segregation in NGC 1805, although these authors assumed that all stars in their sample were single stars. They pointed out that it is not straightforward to correct the observed LF for the presence of binaries, in particular since the binary fraction as a function of brightness is difficult to determine. Note that, despite significant progress and improvements, here we still can only determine the binary fraction for cluster MS stars spanning a narrow mass range (roughly for  $m_* \in [1.3 M_\odot, 1.9 M_\odot]$ , corresponding to F-type primary stars).

To understand the radial dependence of the binary fraction of F-type stars in NGC 1805, we need to compare the time-scale governing early dynamical mass segregation with the cluster's age. de Grijs et al. (2002b) calculated that the core of NGC 1805 is 3–4 crossing times old, although they adopted a chronological age of  $\log(t/\text{yr}) = 7.0^{+0.3}_{-0.1}$ . Since the age we adopted is older, this implies that the cluster age in units of the crossing time reported in de Grijs et al. (2002b) is a lower limit. In fact, adopting an age of  $\log(t/\text{yr}) = 7.65 \pm 0.10$ , we estimate that the core of NGC 1805 may be of order 8–10 crossing times old. In addition, Allison et al. (2009, 2010) pointed out that if – as suggested by observations – clusters form clumpy rather than as spherically homogeneous Plummer spheres (see also Moeckel & Bonnell 2009), they will undergo early dynamical mass segregation more quickly, on time-scales of 1–2 Myr for the most massive stars in the cores of their open cluster-like model systems (for an alternative scenario leading to rapid mass segregation, see McMillan et al. 2012). In view of these time-scale arguments and compared with the cluster's chronological age, its binary population should have been modified by dynamical interactions.

Binary systems can be formed through both three-body

encounters ('3b') and tidal capture ('tc'; Spitzer 1987), i.e.,

$$\left(\frac{dn_b}{dt}\right)_{\text{tot}} = \left(\frac{dn_b}{dt}\right)_{3b} + \left(\frac{dn_b}{dt}\right)_{\text{tc}}. \quad (5)$$

Spitzer (1987) provides a useful numerical approximation to the formation rate of binaries through three-body encounters,

$$\begin{aligned} \left(\frac{dn_b}{dt}\right)_{3b} &= 1.97 \times 10^{-13} \left(\frac{n}{10^4 \text{ pc}^{-3}}\right)^3 \left(\frac{m_*}{M_\odot}\right)^5 \\ &\times \left(\frac{10 \text{ km s}^{-1}}{\sigma_{m_*}}\right)^9 \text{ pc}^{-3} \text{ yr}^{-1}, \end{aligned} \quad (6)$$

where  $n$  and  $\sigma_{m_*}$  are the stellar density and 3D velocity dispersion of single stars, respectively. For the rate of binary formation through tidal capture, we have

$$\begin{aligned} \left(\frac{dn_b}{dt}\right)_{\text{tc}} &= 10^{-8} \kappa \left(\frac{n}{10^4 \text{ pc}^{-3}}\right)^2 \left(\frac{m_*}{M_\odot}\right)^{1+\mu/2} \\ &\times \left(\frac{R_s}{R_\odot}\right)^{1-\mu/2} \left(\frac{10 \text{ km s}^{-1}}{\sigma_{m_*}}\right)^{1+\mu} \text{ pc}^{-3} \text{ yr}^{-1}. \end{aligned} \quad (7)$$

Here,  $(\kappa, \mu) = (1.52, 0.18)$  and  $(2.1, 0.12)$  for the polytropes  $n = 3$  (resulting from the Eddington standard model of stellar structure for MS stars) and 1.5 (relevant to degenerate stellar cores, white dwarfs and less massive bodies), respectively, and  $R_s$  is the stellar radius.

Let us now estimate the number of binaries that may have formed through tidal capture during the lifetime of NGC 1805. Mackey & Gilmore (2003) determined a (central) density of  $\log \rho_0 [M_\odot \text{ pc}^{-3}] = 1.75 \pm 0.06$  and a total mass of  $\log(M_{\text{cl}}/M_\odot) = 3.45^{+0.10}_{-0.11}$  for this cluster. Within a radius of  $45''$ , which roughly corresponds to the size of NGC 1805 (see Table 2), we detected 3500 stars. Corrected for incompleteness,<sup>4</sup> We now simply assume that this sample represents the total number of cluster members, so that the average stellar mass in the cluster is of order  $0.28 M_\odot$ .<sup>5</sup> This corresponds to a central number density of  $\rho = 70$  stars  $\text{pc}^{-3}$ , assuming that the average mass of stars for  $V \in [20.5, 22.0]$  mag is  $1.6 M_\odot$ . MS stars in this mass range have radii of roughly  $1.3 R_\odot$ ; the cluster's stellar velocity dispersion is still unknown. de Grijs et al. (2002b) estimated that the velocity dispersion of NGC 1805 should be more than 10 times smaller than that of NGC 1818, while Elson et al. (1987) estimated a velocity dispersion for NGC 1818 of  $\geq 6.8 \text{ km s}^{-1}$ . We hence simply assume a velocity

<sup>4</sup> The completeness level sharply decreases near  $V = 24.0$  mag. For fainter stars, we assume a Kroupa (2001)-like LF shape down to the hydrogen-burning limit at  $0.1 M_\odot$ . This shape is, to first order, appropriate for both NGC 1805 and NGC 1818 (cf. Liu et al. 2009a,b). we estimate that NGC 1805 contains a total of approximately 10,000 stars

<sup>5</sup> It is encouraging – and instills confidence in our results – that the cluster masses implied by simply adding up the individual stellar masses obtained from integrating both clusters' stellar mass functions over the full mass range, including the uncertain extrapolation to lower stellar masses, are similar to the cluster masses reported in the literature, at least to first order. Here, we derive cluster masses for NGC 1805 and NGC 1818 of  $\log(M_{\text{cl}}/M_\odot) \sim 3.8$  and 4.0, respectively, which must be compared with  $\log(M_{\text{cl}}/M_\odot) = 3.45^{+0.10}_{-0.11}$  and  $4.01 \pm 0.10$ , respectively, from Mackey & Gilmore (2003).

dispersion for NGC 1805 of  $\sim 0.7 \text{ km s}^{-1}$ . Also, we adopt 5 arcsec as projected core size of NGC 1805, which roughly corresponds to 1.3 pc at the distance of the LMC. These considerations imply that, by the cluster’s current age, only 5.6 and 0.2 binaries are expected to have formed in the cluster core through three-body encounters and tidal capture, respectively.

NGC 1805 exhibits a significantly decreasing binary fraction out to  $R = 15$  arcsec. Since Mackey & Gilmore (2003) determined a cluster core radius of  $5.47 \pm 0.23$  arcsec, this decreasing trend covers up to 3 core radii. We do not explore the binary fraction in the innermost 5 arcsec because of the large uncertainties associated with the small number of stars in that region. Nevertheless, it is still reasonable to conclude that the higher binary fraction in the cluster’s inner region is most likely due to the effects of early dynamical mass segregation (cf. Allison et al. 2009, 2010), a process akin to violent relaxation. After all, binary systems are, on average, more massive than the single stars they are composed of, so that they are subject to a more significant degree of dynamical friction and, hence, mass segregation.

In addition, as the more massive stars sink towards the cluster centre, their dynamical evolution speeds up (Gurkan et al. 2004). This will be accelerated if – as usual in realistic star clusters – there is no full energy equipartition (Inagaki & Saslaw 1985), thus producing high-density cores very rapidly, where stellar encounters occur very frequently and binary formation is thought to be very effective (Inagaki & Saslaw 1985; Elson et al. 1987). In fact, the presence of binary stars may accelerate this early dynamical mass segregation significantly, since two-body encounters are very efficient (Nemeč & Harris 1987; De Marchi & Paresce 1996; Bonnell & Davies 1998; Elson et al. 1998; Parker et al. 2009). This process will act on similar (or slightly shorter) time-scales as conventional dynamical mass segregation, which occurs through standard two-body relaxation.

### 5.3.2 Binary dynamical disruption

Since NGC 1818 has a similar age as NGC 1805, the opposite behaviour of the radial binary fraction seen for NGC 1818 indicates that additional dynamical effects may also play an important role. In de Grijs et al. (2013), we concluded that the apparent deficit of binaries in the NGC 1818 core may be the observational signature of the preferential disruption of soft binary systems. In this paper, our improved  $\chi^2$ -minimization procedure has yielded an even more robust increasing trend for NGC 1818’s radial binary fraction than that reported by de Grijs et al. (2013). This thus underscores our earlier conclusion.

In massive star clusters, hard binaries get harder, on average, and soft binaries become softer (Heggie 1975; Binney & Tremaine 1987). In addition, Binney & Tremaine (1987) point out that the time-scale governing soft binary systems should always be significantly shorter than the local relaxation time-scale. This implies that if there are sufficient numbers of soft binary systems and the cluster has undergone evolution for longer than its half-mass relaxation time, binary disruption should have proceeded efficiently.

de Grijs et al. (2002b) calculated an age of NGC 1818’s core of  $\geq 5$ –30 crossing times, which compares favourably

with our age estimate of the NGC 1805 core, also in units of crossing times. Both clusters have similar chronological ages, yet their binary fractions’ radial profiles are markedly different. What causes this apparent diversity? Disruption of binary systems is driven by kinetic-energy transfer from a cluster’s bulk stars to the binary members of interest. Once the velocities of the binary components are much lower than those of the bulk stellar population, such a binary system can be treated as soft. Binney & Tremaine (1987) derived the ‘watershed’ energy of soft binaries as  $-m\sigma^2$ , where  $\sigma$  is the local velocity dispersion of the environment in which the binaries reside. Since the mass ranges of the binaries we analysed in both NGC 1805 and NGC 1818 are similar, the main factor which determines if a binary system is a soft binary system is its velocity dispersion. Since de Grijs et al. (2002b) suggested that the velocity dispersion of the NGC 1818 core may be roughly 10 times greater than that of the core of NGC 1805, many more binaries in NGC 1818 are thought to be soft binaries. They are more easily disrupted in the dense core of NGC 1818, while such binary systems are likely to survive more easily in NGC 1805. In addition, NGC 1818 also has a relatively denser core compared with NGC 1805. Sollima (2008; his fig. 6) derived a relationship between the survival frequency of binary systems and the density and velocity dispersion of their host clusters, which shows that binaries survive much more easily in environments characterized by relatively low densities and velocity dispersions. We speculate that these differences in physical conditions are at the basis of the significantly different radial binary fraction profiles observed for both clusters.

Let us now adopt velocity dispersions for NGC 1805 and NGC 1818 of 7 and  $0.7 \text{ km s}^{-1}$ , respectively, and total masses of  $\log(M_{\text{cl}}[M_{\odot}]) = 3.45_{-0.11}^{+0.10}$  and  $4.01 \pm 0.10$ . Corrected for incompleteness, we concluded that of order 10,000 stars are likely associated with NGC 1805 within a radius of 45 arcsec; for NGC 1818 we estimate a total stellar membership count of 14,500 stars within 73.7 arcsec. We hence adopt the simple assumption that NGC 1805 (NGC 1818) is composed of 10,000 (14,500) stars, which allows us to derive an average stellar mass of  $\bar{m} = 0.28_{-0.06}^{+0.07} (0.71_{-0.15}^{+0.18}) M_{\odot}$ . These values allow us to estimate the typical semi-major axis length of the binary systems in both clusters,

$$a = \frac{G\bar{m}}{2\sigma^2} \quad (8)$$

where  $G$  is the gravitational constant and  $\sigma$  is the cluster’s velocity dispersion. For binary systems to survive for a significant period of time in the cluster centre, the typical minimum semi-major axis required for NGC 1805 is of order 250 au, while that for NGC 1818 is only  $\sim 6$  au. Duquennoy & Mayor (1991) systematically explored the properties of the binarity and higher-order multiplicity of stars in the solar neighbourhood. They found for nearby field binary systems that the distribution of their typical semi-major axes peaks at 30 au. If we adopt the simplistic assumption that the same solar-neighbourhood conditions also apply to the LMC field, this may indicate a medium value for the semi-major axes of surviving binaries.

These arguments thus support the notion that relatively wide binaries are more easily disrupted in the environment of the NGC 1818 core. This also corroborates the idea that dynamical evolution is likely to have acted on the stars in

the core of NGC 1818, but also in NGC 1805 (although to a lesser degree). In turn, this is underscored by the results of de Grijs et al. (2002a,b), who found significant mass (luminosity) segregation of the single stars in both clusters out to several core radii. Note that these authors did not correct their results for binarity, although the bulk ( $\gtrsim 60$  per cent) of their sample stars would have been single stars. Combined with recent insights into rapid dynamical evolution in initially cool cluster cores (e.g. Allison et al. 2009, 2010), this suggests that at least some of the observed degree of mass segregation may be dynamical in origin.

## 6 CONCLUSIONS

In this paper, we have used isochrone fitting and  $\chi^2$  minimization to investigate the binary fractions as a function of radius in the young massive LMC star clusters NGC 1805 and NGC 1818. Both methods agree very well with one another as regards the radial trends of the clusters' binary fractions. This implies that both approaches yield robust results.

Our scientific results exhibit opposite trends regarding the behaviour of the binary fractions as a function of radius in the inner regions of both clusters. For NGC 1805, we detected a significant decrease in the binary fraction from the inner core to the cluster's periphery. Meanwhile, for NGC 1818 we found a monotonic increase of the binary fraction with radius. We conclude that while early dynamical mass segregation and the disruption of soft binary systems should be at work in both clusters, time-scale arguments imply that early dynamical mass segregation should be very efficient and, hence, likely dominates the dynamical processes in the core of NGC 1805. Meanwhile, in NGC 1818 the behaviour in the core is probably dominated by disruption of soft binary systems. We speculate that this may be owing to the higher velocity dispersion in the NGC 1818 core, which creates an environment in which the efficiency of binary disruption is high compared with that of the NGC 1805 core.

## ACKNOWLEDGMENTS

We are grateful for support from the National Natural Science Foundation of China through grants 11073001 and 10973015.

## REFERENCES

- Allison R. J., Goodwin S. P., Parker R. J., de Grijs R., Portegies Zwart S. F., Kouwenhoven M. B. N., 2009, *ApJL*, 700, L99
- Allison R. J., Goodwin S. P., Parker R. J., Portegies Zwart S. F., de Grijs R., 2010, *MNRAS*, 407, 1098
- Avni Y., 1976, *ApJ*, 210, 642
- Bailyn C. D., Sarajedini A., Cohn H., Lugger P. M., Grindlay J. E., 1992, *ApJ*, 103, 5
- Baraffe I., Chabrier G., Allard F., Hauschildt P. H., 1998, *A&A*, 337, 403
- Bastian N., de Mink S. E., 2009, *MNRAS*, 398, L11
- Bate M. R., 2009, *MNRAS*, 392, 590
- Binney J., Tremaine S., 1987, *Galactic Dynamics*, p. 526ff, Princeton: Princeton Univ. Press
- Bonnell I. A., Davies M. B., 1998, *MNRAS*, 295, 691
- Bressan A., Marigo P., Girardi L., et al., 2012, *MNRAS*, 427, 127
- Castro R., Santiago B. X., Gilmore G. F., Beaulieu S., Johnson R. A., 2001, *MNRAS*, 326, 333
- de Grijs R., Johnson R. A., Gilmore G. F., Frayn C. M., 2002a, *MNRAS*, 331, 228
- de Grijs R., Gilmore G. F., Johnson R. A., Mackey A. D., 2002b, *MNRAS*, 331, 245
- de Grijs R., Gilmore G. F., Mackey A. D., et al., 2002c, *MNRAS*, 337, 597
- de Grijs R., Li C., Zheng Y., et al., 2013, *ApJ*, 765, 4
- De Marchi G., Paresce F., 1996, *ApJ*, 467, 658
- Dolphin A. E., 2000, *PASP*, 112, 1383
- Dolphin A. E., 2005, *HSTphot User's Guide*, v. 1.1.7b (<http://purcell.as.arizona.edu/hstphot/>)
- Duquennoy A., Mayor M., 1991, *A&A*, 248, 485
- Elson R. A. W., Hut P., Inagaki S., 1987, *ARA&A*, 25, 565
- Elson R. A. W., Sigurdsson S., Davies M., Hurley J., Gilmore G., 1998, *MNRAS*, 300, 857
- Girardi L., Rubele S., Kerber L., 2009, *MNRAS*, 394, L74
- Griffin R. F., Suchkov A. A., 2003, *ApJS*, 147, 103
- Gurkan M. A., Freitag M., Rasio F. A., 2004, *ApJ*, 604, 632
- Halbwachs J. L., Mayor M., Udry S., Arenou F., 2003, *A&A*, 397, 159
- Heggie D. C., 1975, *MNRAS*, 173, 729
- Hu Y., Deng L., de Grijs R., Liu Q., Goodwin S. P., 2010, *ApJ*, 724, 649
- Hu Y., Deng L., de Grijs R., Liu Q., 2011, *PASP*, 123, 107
- Hunter D. A., Light R. M., Holtzman J. A., et al., 1997, *ApJ*, 478, 124
- Inagaki S., Saslaw W. C., 1985, *ApJ*, 292, 339
- Ivanova N., Belczynski K., Fregeau J. M., Rasio F. A., 2005, *MNRAS*, 358, 572
- Javiel S. C., Santiago B. X., Kerber L. O., 2005, *A&A*, 431, 73
- Johnson R. A., Beaulieu S. F., Gilmore G. F., et al., 2001, *MNRAS*, 324, 367
- Kaczmarek T., Olczak C., Pfalzner S., 2011, *A&A* 528, A144
- Kerber L. O., Santiago B. X., 2005, *A&A*, 435, 77
- Kouwenhoven M. B. N., Brown A. G. A., Zinnecker H., Kaper L., Portegies Zwart S. F., 2005, *A&A*, 474, 77
- Kouwenhoven M. B. N., Brown A. G. A., Portegies Zwart S. F., Kaper L., 2007, *A&A*, 474, 77
- Kroupa P., 2001, *MNRAS*, 322, 231
- Lada C. J., Lada E. A., 2003, *ARA&A*, 47, 57
- Li C., de Grijs R., Deng L., Liu X. K., 2013, *ApJL*, 770, L7
- Li Z., Mao C., Li C., Zhang Q., 2012, *ApJ*, 761, L22
- Liu Q., de Grijs R., Deng L., Hu Y., Baraffe I., Beaulieu S. F., 2009a, *MNRAS*, 396, 1665
- Liu Q., de Grijs R., Deng L., Hu Y., Beaulieu S. F., 2009b, *A&A*, 503, 469
- Mackey A. D., Gilmore G. F., 2003, *MNRAS*, 338, 85
- Mackey A. D., Broby Nielsen P., 2007, *MNRAS*, 379, 151
- Mackey A. D., Broby Nielsen P., Ferguson, A. M. N., Richardson J. C., 2008, *ApJ*, 681, L17
- Mateo M., 1996, in: *The origins, evolution, and destinies of*

binary stars in clusters (Milone E. F., Mermilliod, J.-C., eds.), ASP Conf. Ser., 90, 21

McMillan S., Vesperini E., Kruczek N., 2012, *Highlights of Astronomy*, in press (arXiv:1210.8200)

Milone A. P., Bedin L. R., Piotto G., Anderson J., 2009, *A&A*, 497, 755

Milone A. P., Bedin L. R., Aparicio A., et al., 2012, *A&A*, 540, A16

Moeckel N., Bonnell I. A., 2009, *MNRAS*, 396, 1874

Nemec J. M., Harris H. C., 1987, *ApJ*, 316, 172

Parker R. J., Goodwin S. P., Kroupa P., Kouwenhoven M. B. N., 2009, *MNRAS*, 397, 1577

Rastegaev D. A., 2010, *AJ*, 140, 2013

Reggiani M. M., Meyer M. R., 2011, *ApJ*, 738, 60

Rubenstein E. P., Bailyn C. D., 1997, *ApJ*, 474, 701

Santos J. F. C. Jr, Dottori H., Grosbøl P., 2013, *A&A*, 553, A74

Sollima A., Beccari G., Ferraro F. R., Pecci Fusi F., Sarajedini A., 2007, *MNRAS*, 380, 781

Sollima A., 2008, *MNRAS*, 388, 307

Sollima A., Carballo-Bello J. A., Beccari G., et al., 2010, *MNRAS*, 401, 577

Spitzer L. Jr, 1987, *Dynamical Evolution of Globular Clusters*, Princeton: Princeton Univ. Press

Trenti M., Heggie D. C., Hut P., 2007a, *MNRAS*, 374, 344

Trenti M., Ardi E., Mineshige S., Hut P., 2007b, *MNRAS*, 374, 857

Wall J. V., 1996, *QJRAS*, 37, 519

Will J.-M., Bomans D. J., Tucholke H.-J., et al., 1995, *A&AS*, 112, 367

Yang W., Bi S., Meng X., Liu Z., 2013, *ApJ*, submitted (arXiv:1304.5865)

Zhao B., Bailyn C. D., 2005, *AJ*, 129, 1934

## APPENDIX

In this Appendix, we further compare the quality and accuracy of the completeness curves for both NGC 1805 and NGC 1818 obtained using both simulated AS tests based on catalogue data (Hu et al. 2010, 2011) and ‘real’ (actual) AS tests as employed in this paper. We added ‘real’ ASs to the reduced images using the *HSTPHOT* package, which can generate ASs that resemble real objects as observed with the *HST*/WFPC2 camera.

Hu et al. (2011) claimed that on the basis of their catalogue-based method, they can very well reproduce the NGC 1818 completeness curve, as if they had employed actual AS tests. However, they only show the completeness curve for the WFPC2/WF3 chip. On close inspection, we found that their results may only be correct for the relatively low-density environments for which they carried out their comparison. We repeated their catalogue-based and our actual AS tests using our NGC 1805 data, and indeed found excellent agreement between both completeness curves in the low-density regions on the WFPC2 (WF3) chips.

However, if we consider more crowded regions, the incompleteness levels resulting from the actual AS tests are significantly lower than those from the catalogue-based method of Hu et al. (2011). Figures 19 and 20 show the completeness curves of the four WFPC2 chips for the NGC 1805 and NGC 1818 data, respectively. This result implies

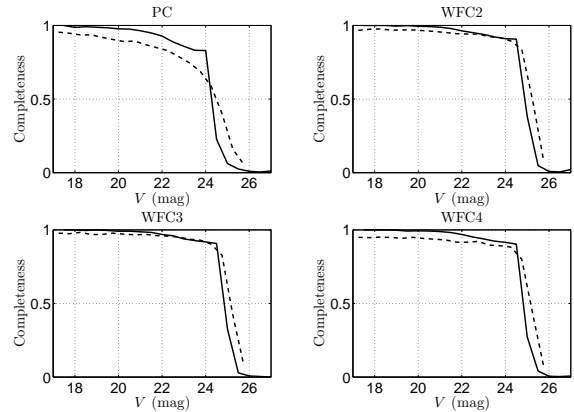


**Figure 19.** Completeness curves for the NGC 1805 data for different WFPC2 chips. Dashed, solid lines: Results from the real and catalogue-based (Hu et al. 2011) ASs tests, respectively.

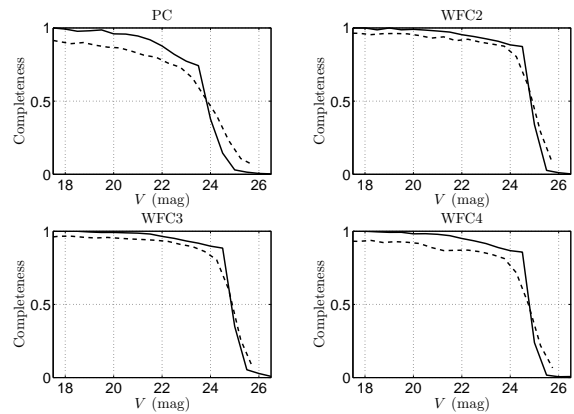


**Figure 20.** As Fig. 19, but for NGC 1818.

that the method proposed by Hu et al. (2011) may only be fully applicable to low-density regions and a one-to-one correspondence breaks down above a certain density threshold. (The actual density threshold for which this statement holds requires in-depth exploration of the data at magnitudes well outside the range considered here for our binarity analysis. This is beyond the scope of the present paper, but will be explored in a future, technical contribution.)

We will now consider the origin of the main differences between both methods. Hu et al. (2011) mainly considered two factors that will affect the incompleteness levels of a data set:

- (i) For bright stars, incompleteness is mainly caused by star–star blends;
- (ii) For faint stars, incompleteness is mainly owing to stars remaining hidden in the background noise or below the background level.

Hu et al. (2011) mention that stars may also blend with bad pixels, cosmic rays and – to a very small extent – background galaxies. They state that these effects render their completeness levels lower than the real completeness level which one could determine on the basis of actual AS tests. We concur with this statement and we also emphasize that



special attention must be paid to saturated stars. The latter objects will dominate the central regions of star cluster observations, where it transpires that genuine stars will likely also blend with the overspill counts (‘bleeding’ across detector rows or columns) caused by saturated pixels. This will further reduce the actual completeness levels of one’s data set in high-density regions where saturated stars may be common.

To explore this effect, we plotted the spatial distribution on the PC chip of all ASs that were added to the NGC 1818 data but which were not recovered by our actual AS tests. We also found that a significant fraction of our source detections in the master catalogue originating from the PC chip had been identified by HSTPHOT as ‘extended’ sources. We became suspicious of the higher-than-expected fraction of such sources and also plotted their distribution across the PC chip. It turns out that this distribution displays a clear pattern which is associated with the distribution of the saturated sources: they trace cross-like patterns on the chip.

In Fig. 21 we show the distribution of both the ‘extended’ sources (red dots) and the ASs which our routines failed to recover (blue dots). Both distributions are clearly similar. This suggests that saturation will lead to enhanced incompleteness levels over and above those expected from crowding and a higher background level in such areas. Since the effects of mass segregation will cause the more massive and, hence, brighter stars to migrate to a cluster’s centre, saturation will most likely disproportionately affect the highest-density cluster core region. Hence, consideration of only real point sources as genuine stars and adoption of a minimum blending distance alone cannot reproduce the actual levels of sampling (in)completeness in the presence of saturated stars. This is why, for our observations on the PC chip, the catalogue-based AS tests yield a significantly higher completeness fraction than that suggested by our actual AS tests. Although the low-density data on the WF3 chip also include a number of saturated stars, their number is much smaller, so that the results from both methods are in much better agreement with one another.

To further test if our conclusions are correct, we adapted the incompleteness criteria of Hu et al. (2011). For stars brighter than the detection limit, these authors assume that in a scenario where a faint star blends with a brighter counterpart, the faint star will not be recovered and only the brighter star is retained in the output catalogue. We extended this criterion to all objects, including the sources erroneously flagged as ‘extended’. No matter how bright the AS is, once it blends with such ‘extended’ sources, it will not be recovered. In other words, even if the ‘extended’ source is fainter than the AS with which it is found to blend, the bright AS will not be recovered, which hence reduces the data set’s inferred completeness levels.

We applied this new approach to the NGC 1818 data on the PC chip, since there our catalogue-based approach most poorly reproduced the completeness curve determined by the actual AS tests. Indeed, we found that after implementation of this correction, the catalogue-based, simulated completeness curves are much closer to the equivalent curves based on the actual AS tests. However, we also noted a relatively larger offset at the faint tail. This may have been caused by the complicated LF on the PC chip due to the dynamical redistribution of stars of different masses which

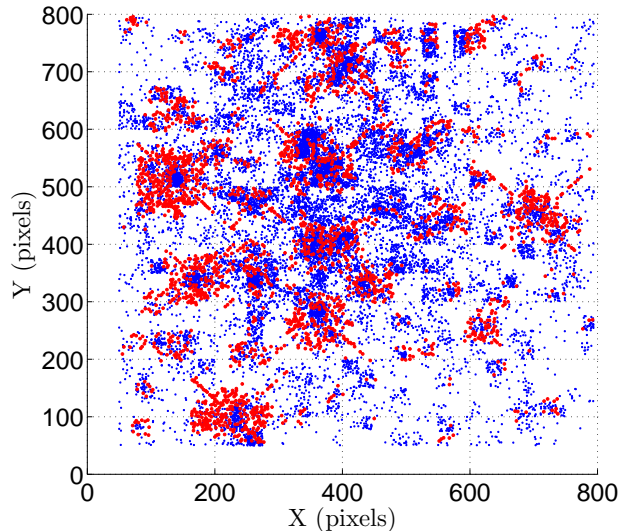


**Figure 21.** Spatial distributions of both the observed ‘extended’ sources (red dots) and the actual ASs which were not recovered by our analysis routines. The cross-like patterns due to saturated stars are clearly discernible.

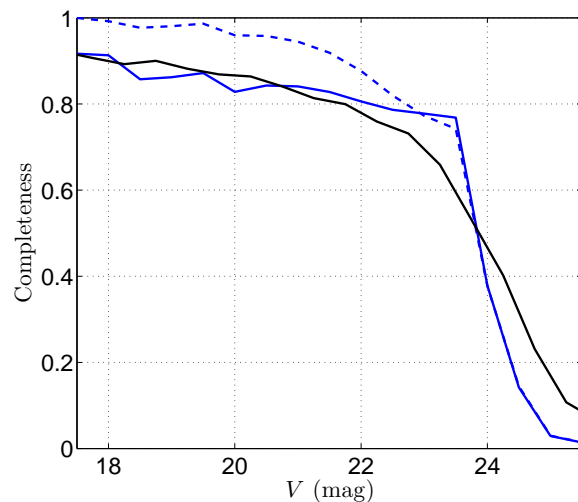


**Figure 22.** Completeness curves based on the simulated AS tests (blue dashed line), the actual AS tests (black solid line) and the simulated AS tests after correction (blue solid line; see text), applied to the NGC 1818 observations on the PC chip.

leads to mass segregation. Figure 22 shows a comparison of the completeness curves based on the simulated (catalogue-based) AS tests (blue dashed line), the actual AS tests (black solid line) and the simulated AS tests after correction (blue solid line), for the PC observations covering NGC 1818. In this paper we use (and correct for) the (in)completeness levels inferred from the actual AS tests.

These results thus support our suggestion that saturated stars may have a disproportionate effect on one’s completeness levels. To prove this beyond doubt, one would need to mask the pattern of saturated stars and repeat the AS tests under different conditions and in areas of different ob-

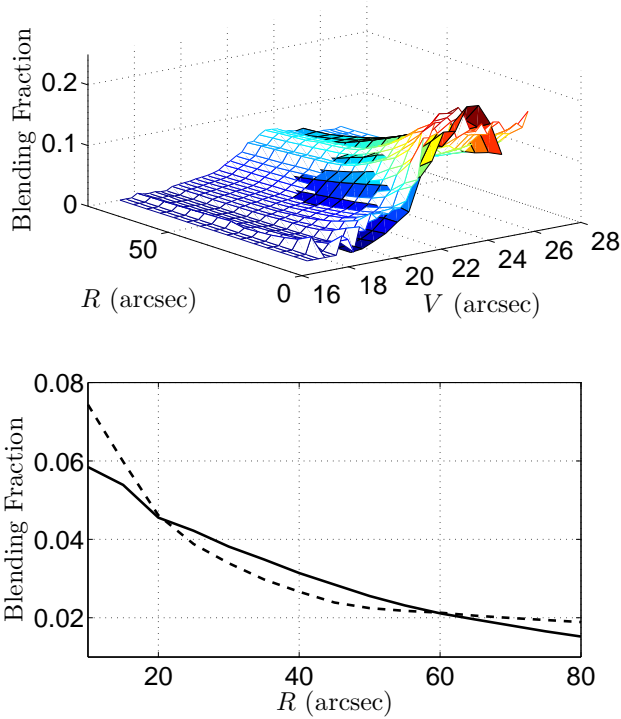


**Figure 23.** (top) 3D surface blending fraction as a function of radius and magnitude. Open, filled grids: Results from the simulated (catalogue-based) and actual AS tests, respectively. (bottom) Blending fraction for all stars with  $V \in [20.5, 22]$  as a function of radius. Typical uncertainties are  $\lesssim 1$  per cent.

ject densities. This is beyond the scope and remit of the present paper, however. We will explore these issues in a future, technical contribution.

Finally, we found that even though the simulated, catalogue-based AS tests may fail to recover the full completeness characteristics in crowded regions, our results regarding the occurrence of optical pairs remain robust and unchanged. (The latter result was based on the approach proposed by Hu et al. 2011.) This is so, because only stars that blend with other stars will produce a ‘blending binary’. Stars which are located close to or on the patterns caused by saturated stars will either not be recovered or be identified as ‘extended’ objects. In either case, these blends are not included in our analysis. The top panel of Fig. 23 compares the 3D blending fraction of NGC 1805 obtained from simulated, catalogue-based AS tests (open grid) with that resulting from the actual AS tests (filled grid). We also show the total blending fraction as a function of radius over the magnitude range of interest in this paper,  $V \in [20.5, 22]$  mag (bottom panel). Given that the typical uncertainties are  $\lesssim 1$  per cent, both distributions are clearly very similar.